Chapter 2
Background on Wireless Communication

2.1 Introduction

In this chapter, we present a brief overview of basic wireless communication systems. The chapter starts with a description of wireless communication channel models including multiple input multiple output (MIMO) channel models and dual-polarized antennas channel models. We then discuss about digital modulation and orthogonal frequency division multiplex (OFDM). Finally, we will provide a short introduction on diversity and spatial multiplexing gain in wireless communication systems and MIMO systems. We will introduce different MIMO space-time block codes (STBC) that will be used in the rest of the book. For a detailed treatment of wireless communication systems we refer to the books of Goldsmith [15], Tse and Viswanath [51] or Molisch [32], Proakis [40].

2.2 Wireless Communication Channel Models

2.2.1 Introduction

Compared to wireline channels, the wireless channels vary over time and frequency depending on the objects surrounding the transmitter, the radiated area and the receiver. The variations of the channel strength can be divided into two classes [41]:

- Large-scale fading: coming from the path loss due to the distance between the transmitter and the receiver (typically higher than 100 m) and the shadowing due to the obstacles (typically few meters to 100 m).
- Small-scale fading: the transmitted signal could arrive at the receiver through multiple paths, which experience different attenuations, arrive at different time delays and phases. It results in constructive or destructive summation of the transmitted signal and causes rapid variations. Furthermore, the path lengths

B. Özbek and D. Le Ruyet, *Feedback Strategies for Wireless Communication*,
DOI 10.1007/978-1-4614-7741-9_2, © Springer Science+Business Media New York 2014

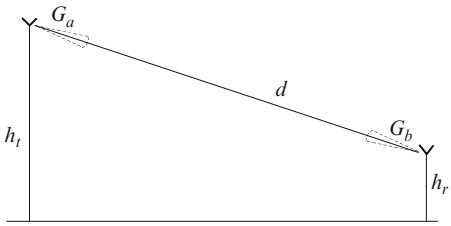

Fig. 2.1 Free space model

and the geometry alter due to the changes in the transmission environment or due to the relative motion of antennas, and the signal level might be subject to fluctuations.

While both classes are important, we will mainly focus on the second class since small-scale fading is more important for the design of feedback strategies in wireless communication systems.

2.2.2 Path Loss and Shadowing

2.2.2.1 Free Space

We first consider a free space transmission between a fixed transmitter and a receiver situated at a distance d from the transmitter as shown in Fig. 2.1.

Let's assume that the transmitted signal is $x(t) = \cos(2\pi f_0 t)$ where f_0 is the carrier frequency. In the far field, the received signal at time t is

$$r(t) = \frac{\lambda\sqrt{G_a G_b}}{4\pi d}\cos\left(2\pi f_0\left(t - \frac{d}{c}\right)\right) \tag{2.1}$$

where G_a and G_b are, respectively, the gain of the transmit and receive antenna in the direction of interest ($G_a = 1$ if the transmit antenna is isotropic), $\lambda = \frac{c}{f_0}$ is the wavelength associated to the carrier frequency f_0 and $c = 3.10^8$ m/s is the speed of light. As expected, in the free space, since the electric field decreases as d^{-1}, the received power decreases as d^{-2}. In this model, the path loss $F_A(d)$ in dB is given by

$$\begin{aligned} F_A(d) &= 10\log_{10}\left(\frac{P_r}{P_t}\right)^{-1} \\ &= 20\log_{10}\left(\frac{4\pi d}{\lambda}\right) - 10\log_{10} G_a G_b \\ &= 32,44 + 20\log_{10} f_0 + 20\log_{10} d - 10\log_{10} G_a G_b \end{aligned} \tag{2.2}$$

A first simple model in mobile radio channel where the pathloss is proportional to d^{α} is given by

$$F_A(d) = -10\log_{10} K_A + 10\alpha \log_{10}\left(\frac{d}{d_0}\right) \tag{2.3}$$

where d_0 is the distance from which the far field assumption is valid. $1 < d_0 < 10$m for indoor systems and $10 < d_0 < 100$ m for outdoor systems. The exponent α range between 1,5 and 6,5. K_A and α can be obtained from measurement campaigns.

Different models are available in the literature and standards depending on the context (macrocell, microcell, picocell, urban, rural, indoor, ...). As an example, for urban applications and considering a frequency range between 150 and 1,500 MHz, we can use the Okumura–Hata model where the empirical pathloss $F_A(d)$ in dB is given by

$$F_A(d)=69.55+26.16\log_{10} f_0-13.82\log_{10} h_t-a(h_r)+(44.9-6.55\log_{10} h_t)\log_{10} d \tag{2.4}$$

where f_0 is the carrier frequency in MHz (150 MHz < f_0 < 1,500 MHz), h_t and h_r are the heights of the transmit and receive antenna, respectively, d is the distance between the transmitter and the receiver in km, and $a(h_r)$ is a correcting factor in dB to take into account the height of the receive antenna given by

$$a(h_r)=\begin{cases}(1.1\log_{10} f_0-0.7)h_r-(1.56\log_{10} f_0-0.8) & \text{small to medium size town}\\ 3.2(\log_{10}(11.75h_r))^2-4.97 & \text{large town}\end{cases} \tag{2.5}$$

The COST 231 models extend the Okumura–Hata model to cover a more elaborated range of frequencies (1.5–2 GHz).

2.2.2.2 Doppler Effect

Let's consider a car equipped with a receive antenna moving in the direction of the transmitter with a speed v as shown in Fig. 2.2.

During Δt, the distance between the transmitter and the receiver decreases by $\Delta d = v\Delta t\cos\theta$ corresponding to a phase shift of $\Delta\phi$

$$\Delta\phi = \frac{v\Delta t\cos\theta}{\lambda}2\pi \tag{2.6}$$

The associated Doppler shift is given by

$$f_D = \frac{vf_0}{c}\cos\theta \tag{2.7}$$

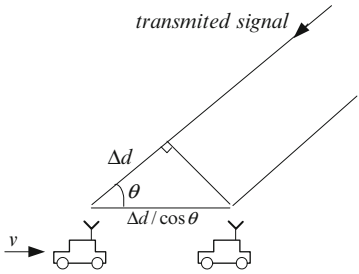

Fig. 2.2 Doppler effect

2.2.2.3 Shadowing

The shadowing effect is due to objects like trees and buildings, obstructing the propagation path between the transmit and the receive antennas. Since the properties of these objects (nature, location, etc.) is not known in advance, we model these properties as a random process. A good approximation of this effect consists in considering that the distribution of the shadow loss ψ is log-normal. The distribution of the logarithm of ψ in dB is Gaussian as follows:

$$p(\psi_{dB}) = \frac{1}{\sqrt{2\pi\sigma^2_{\psi_{dB}}}} \exp\left(- \frac{(\psi_{dB})^2}{2\sigma^2_{\psi_{dB}}} \right) \tag{2.8}$$

where $\psi_{dB} = 10 \log_{10} \psi$ and $\sigma_{\psi_{dB}}$ is the standard deviation of ψ_{dB}. $\sigma_{\psi_{dB}}$ is generally chosen between 5 and 12 dB.

2.2.3 Multipath Channel Models

In wireless communications, multipath fading effect occurs in almost all environment. In urban area where the heights of the mobile antennas are below the height of the surrounding structures there is no line of sight (NLOS) path between the transmitter and the receiver. Thus, the transmitted signal arrives at the receiver through many different paths, reflection, refraction or diffraction over large objects. Multipath fading effects are difficult to predict and consequently they are commonly studied using statistic models. The modeling of multipath fading channels has been established in the early 1960s [3, 7]. We will start by introducing the most general description of the impulse response of the multipath fading channel.

2.2.3.1 General Description

Let $h(\tau, t)$ be the complex envelop of the time-varying channel response where t is the time-varying parameter and τ is the path delay parameter. The envelop $h(\tau, t)$

can be written as the sum of N_p elementary responses with amplitude $\alpha_n(t)$, phase $\phi_n(t)$ and excess time delay $\tau_n(t)$ (each response corresponds to an elementary physical path):

$$h(\tau, t) = \sum_{n=0}^{N_p-1} \alpha_n(t) e^{-j\phi_n(t)} \delta(t - \tau_n) \tag{2.9}$$

where $\delta(t)$ is the Dirac delta function. Hence, a path has zero amplitude for all time delays except $\tau = \tau_n$. The power $\mathbb{E}(\alpha_n^2(t))$ and delay τ_n of each path is determined with the power-delay profile (PDP) which is generally represented as plots of relative received power as a function of delay spread with respect to time.

2.2.3.2 Narrowband Model

In this model, we consider that the delay spread is small compared to the symbol period $x(t - \tau_n) \approx x(t)$. Under this hypothesis, the received signal can be approximated as follows:

$$r(t) = \sum_{n=0}^{N_p-1} \alpha_n(t) e^{-j\phi_n(t)} x(t) \tag{2.10}$$

where

$$\phi_n(t) = 2\pi f_0 \tau_n - 2\pi f_{D_n} t - \phi_0 \tag{2.11}$$

2.2.3.3 Rayleigh Distribution

As the multipath could arrive at the receiver in the same time delay with different phases, the amplitudes of these paths could add constructively or destructively. When the resulting amplitude is zero or near zero, we refer to it as a deep fade.

Moreover, the phase and delay of these paths can change significantly within a short period of time. Hence, the resulting amplitude of the channel at a particular time delay can vary within a short time interval. Since the number of paths is high, using the central limit theorem, the channel impulse response $h(t)$ can be modelled as a complex Gaussian random process. When there is no dominant signal path among all the paths, i.e., when there is NLOS, the amplitude of the channel $|h(t)|$ at any time instant is Rayleigh distributed and the distribution of the phase is uniform over the interval $[0, 2\pi]$.

The Rayleigh distribution is given by

$$p_R(r) = \frac{r}{\sigma^2} \exp\left(- \frac{r^2}{2\sigma^2} \right) \tag{2.12}$$

The square of the amplitude $|h(t)|^2$ is exponentially distributed with density

$$p_S(s) = \frac{1}{\sigma^2} \exp\left(- \frac{s}{\sigma^2} \right) \tag{2.13}$$

When there is a direct link between the transmit and receive antennas, i.e. when there is a line of sight (LOS), the received signal equals the superposition of a complex Gaussian component and an LOS component. The amplitude of the channel is modeled using Rician distribution and is correspondingly named the Rician fading channel. The Rician distribution is given by

$$p_R(r) = \frac{r}{\sigma^2} \exp\left(- \frac{r^2 + s^2}{2\sigma^2} \right) I_0\left(\frac{r \times s}{\sigma^2} \right) \tag{2.14}$$

where $I_0(.)$ is the modified Bessel function of the first kind with order zero. The Rician distribution is often described with the fading parameter $K_R = s^2/2\sigma^2$.

2.2.3.4 Autocorrelation and Uniform Scattering Environment Model

Let's assume that the path amplitudes $\alpha_n(t)$ are slowly varying such that we can consider them as constants during the observation time: $\alpha_n(t) \approx \alpha_n$. Under this assumption, the autocorrelation of $h^R(t)$, the real part of $h(t)$, can be written as:

$$\begin{aligned} R_{h^R,h^R}(\tau, t) &= \mathbb{E}(h^R(t) h^R(t+\tau)) \\ &= 0.5 \sum_{n=0}^{N_p - 1} \mathbb{E}(\alpha_n^2) \cos(2\pi f_{Dn} \tau) \end{aligned} \tag{2.15}$$

We can see that $R_{h^R,h^R}(\tau, t)$ is independent of t: $R_{h^R,h^R}(\tau, t) = R_{h^R,h^R}(\tau)$

In Jakes' model [18], it is assumed that the reflectors are uniformly distributed around the receiver as shown in Fig. 2.3. The angle of arrival (AoA) of the N_p paths is $\theta_n = n\Delta\theta$ where $\Delta\theta = 2\pi/N_p$. We also assume that the average channel gain is constant $\mathbb{E}(\alpha_n^2) = 2/N_p$.

Since $f_{Dn} = v cos\theta_n/\lambda$, we have

$$R_{h^R,h^R}(\tau) = \frac{1}{N_p} \sum_{n=0}^{N_p - 1} \cos\left(2\pi \frac{v\tau}{\lambda} \cos\theta_n \right) \tag{2.16}$$

When $N_p \to \infty$, $\Delta\theta \to 0$, by replacing the summation by an integration we obtain

$$\begin{aligned} R_{h^R,h^R}(\tau) &= \frac{1}{2\pi} \int_0^{2\pi} \cos\left(2\pi \frac{v\tau}{\lambda} \cos\theta \right) d\theta \\ &= J_0(2\pi f_D \tau) \end{aligned} \tag{2.17}$$

Fig. 2.3 Jakes' model

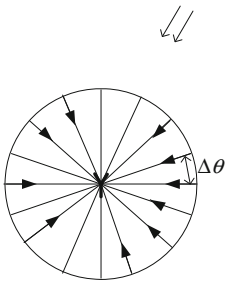

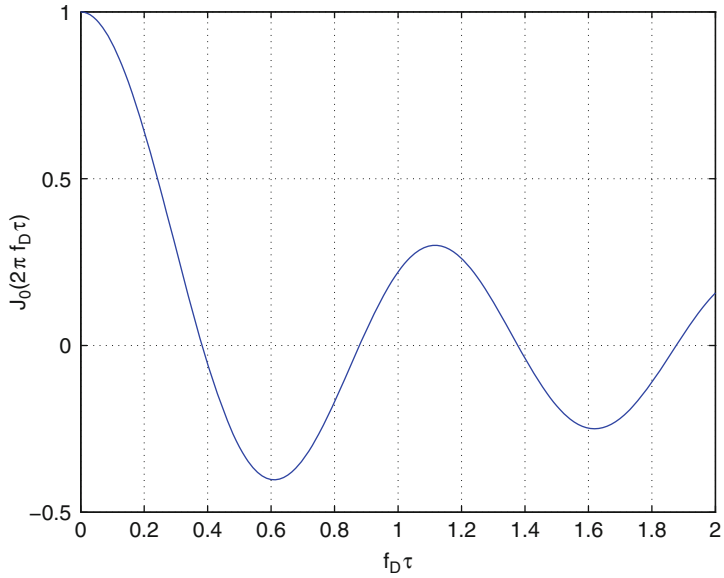

Fig. 2.4 Function $J_0(2\pi f_D \tau)$

where

$$J_0(x) = \frac{1}{\pi} \int_0^{\pi} \exp(-jx \cos\theta) d\theta \tag{2.18}$$

is the Bessel function of first kind and zeroth order as shown in Fig. 2.4 and f_D is the maximum Doppler spread $f_D = v/\lambda$.

The spectrum density of $h^R(t)$ and $h^I(t)$ is obtained by taking the Fourier transform of the autocorrelation

$$S_{h^R,h^R}(f) = S_{h^I,h^I}(f) = \begin{cases} \frac{1}{2\pi f_D} \frac{1}{\sqrt{1-(f/f_D)^2}} & \text{if} \quad |f| \leq f_D \\ 0 & \text{else} \end{cases} \tag{2.19}$$

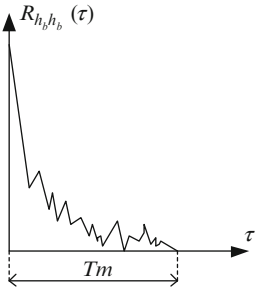

Fig. 2.5 Example of power delay profile

2.2.3.5 Wideband Model

In this section, we consider the general case where the signals are wideband. In this case, the maximum delay spread T_M is higher than the symbol period T_S. The approximation $x(t - \tau_n(t) \approx x(t)$ is no longer valid. Therefore, the received signal is composed of a sum of copies of the transmitted signal where each copy is shifted in phase by $\phi_n(t)$ and delayed by $\tau_n(t)$.

Like previously, $h(\tau, t)$ is random due to the random variability of the phase, amplitude and delay of the different paths. The statistical properties of $h(\tau, t)$ are obtained from the autocorrelation function. Since the channel is usually wide-sense stationary (WSS), the autocorrelation is independent of t. Furthermore, the responses associated to the different delays are uncorrelated since they come from different scatterers. We say that this channel has wide-sense stationary uncorrelated scattering (WSSUS).

Then we have

$$R_{h,h}(\tau, \Delta t) = \mathbb{E}[h^*(\tau_1, t)h(\tau_2, t + \Delta t)] \tag{2.20}$$

with $\tau = \tau_1 - \tau_2$.

The scattering function is defined as the Fourier transform of $R_{h,h}(\tau, \Delta t)$ with respect to Δt:

$$S_{H,H}(\tau, \lambda) = \int_{-\infty}^{+\infty} R_{h,h}(\tau, \Delta t) \exp(-j 2\pi\lambda \Delta t) d\Delta t \tag{2.21}$$

If we let $\Delta t = 0$ in $R_{h,h}(\tau, \Delta t)$, the resulting autocorrelation is the multipath intensity profile or the PDP $R_{h,h}(\tau)$ of the channel

$$R_{h,h}(\tau) \equiv R_{h,h}(\tau, 0) \tag{2.22}$$

The PDP is the average power output of the channel as a function of the delay τ. An example of PDP is given in Fig. 2.5.

From the delay profile, we can compute the maximum delay spread T_M, the mean delay μ_{T_M} and the root mean square delay spread σ_{T_M}.

$$\mu_{T_M} = \frac{\int_0^\infty \tau R_{h,h}(\tau) d\tau}{\int_0^\infty R_{h,h}(\tau) d\tau} \tag{2.23}$$

$$\sigma_{T_M} = \sqrt{\frac{\int_0^\infty (\tau - \mu_{T_M})^2 R_{h,h}(\tau) d\tau}{\int_0^\infty R_{h,h}(\tau) d\tau}} \tag{2.24}$$

2.2.3.6 Delay Spread and Coherence Bandwidth

The time-varying channel can also be characterized in the frequency domain by taking the Fourier transform of $h(\tau, t)$ with respect to τ denoted $H(f, t)$ and given as follows:

$$H(f,t) = \int_{-\infty}^{+\infty} h(\tau, t) \exp(-j2\pi f \tau) d\tau \tag{2.25}$$

As seen previously, for $h(\tau, t)$, $H(f, t)$ is the summation of complex Gaussian random variables and can be described using its autocorrelation function

$$R_{H,H}(\Delta f, \Delta t) = \mathbb{E}[H^*(f_1, t) H(f_2, t + \Delta t)] \tag{2.26}$$

with $\Delta f = f_2 - f_1$.

Again, if we let $\Delta t = 0$ in $R_{H,H}(\Delta f, \Delta t)$,

$$R_{H,H}(\Delta f) \equiv R_{H,H}(\Delta f, 0) \tag{2.27}$$

Since we have

$$R_{H,H}(\Delta f) = \int_{-\infty}^{+\infty} R_{h,h}(\tau) \exp(j2\pi \Delta f \tau) d\tau \tag{2.28}$$

$R_{H,H}(\Delta f)$ is the Fourier transform of the PDP.

The coherence bandwidth B_{coh} can be defined as the range of frequencies over which the amplitude of the spectral components of the channel response are correlated or equivalently for which $R_{H,H}(\Delta f)$ is different from 0. If we relax the constraint to ensure that the frequency correlation function is above 0.5, the coherence bandwidth can be defined as a function of the root mean squared delay spread σ_{T_M} as follows:

$$B_{coh} = \frac{0.2}{\sigma_{T_M}} \tag{2.29}$$

The delay spread of the multipath causes time dispersion of the transmitted signal. Depending on the delay spread and the symbol transmission time T_s, the channels can be categorized as flat fading or frequency selective fading channels.

Flat fading or non-frequency-selective assumption implies that the signal bandwidth B_W is much less than the channel coherence bandwidth B_{coh}. For perfect Nyquist pulses we have $B_W = 1/T_s$ and consequently the flat fading assumption implies that $T_s >> \sigma_{T_M}$.

When the bandwidth of constant amplitude and linear phase response of the channel is significantly less than the transmitted signal bandwidth ($B_{coh} << B_W$), the spectral characteristic of the signal cannot be maintained and the channel becomes frequency selective. In this case, the channel applies different gains or attenuations to different frequency components of the transmitted signal, causing spectral distortion in the signal. In the time domain, the time dispersion of the multipath channel is large enough such that some multipaths can be resolved at the receiver into symbol-spaced delay. In other words, a frequency selective fading channel creates inter symbol interference (ISI) onto the transmitted symbols.

2.2.3.7 Doppler Spread and Coherence Time

The Doppler effect can be seen by taking the Fourier transform of $R_{H,H}(\Delta f, \Delta t)$ relative to Δt:

$$S_{H,H}(\Delta f, \lambda) = \int_{-\infty}^{+\infty} R_{H,H}(\Delta f, \Delta t) \exp(-j 2\pi \lambda \Delta t) d\Delta t \tag{2.30}$$

From $S_{H,H}(\Delta f, \lambda)$, if we set $\Delta f = 0$, it is possible to evaluate the Doppler power spectrum of the channel $S_{H,H}(\lambda) \equiv S_{H,H}(0, \lambda)$

$$S_{H,H}(\lambda) = \int_{-\infty}^{+\infty} R_{H,H}(\Delta t) \exp(-j 2\pi \lambda \Delta t) d\Delta t \tag{2.31}$$

The function $S_{H,H}(\lambda)$ gives the signal intensity as a function of the Doppler frequency λ. The range of values of λ over which $S_{H,H}(\lambda)$ is nonzero is called the Doppler spread f_D. The Doppler spread measures the spectral broadening caused by the rate of change of the channel. As a time domain dual of the Doppler spread, coherence time measures the rate of change of the channel. We define the coherence time T_{coh} as the time during which $R_{H,H}(\Delta t)$ is above 0.5

$$T_{coh} = \sqrt{\frac{9}{16\pi f_D^2}} \tag{2.32}$$

By using this coherence time, the multipath fading channels can be categorized into the fast or slow fading channels. While there is no consensus on those

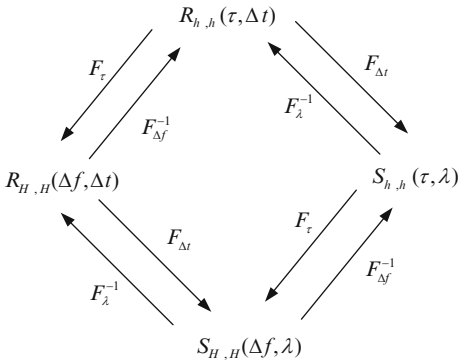

Fig. 2.6 Relationship between the different functions

Table 2.1 ITU pedestrian A channel model for urban environment and 3 km/h mobile speed four multipaths with Rayleigh fading channel

Path	1	2	3	4
Delay (ns)	0	110	190	410
Attenuation (dB)	0	−9.7	−19.2	−22.8

Table 2.2 ITU vehicular A channel model for vehicular with low delay spread and 60 km/h mobile speed six multipaths with Rayleigh fading channel

Path	1	2	3	4	5	6
Delay (ns)	0	310	710	1090	1730	2510
Attenuation (dB)	0	−1	−9	−10	−15	−20

definitions, in this book we will call a channel slow fading if the condition $T_s << T_{coh}$ is satisfied. Since the time during which the channel remains correlated is long compared to the symbol duration, it is expected that the channel is unchanged while the symbol is transmitted. Conversely, if the condition $T_s >> T_{coh}$ is satisfied, the channel is said to be fast fading since the fading characteristics of the channel change while transmitting the symbol. Depending on the channel variation, we will consider ergodic capacity (fast fading channel) or outage capacity (slow fading channel) which will be presented later. As a conclusion, delay spread, coherence bandwidth, Doppler spread and coherence time can be derived from four different functions as depicted in Fig. 2.6.

Two examples of multipath fading channel models are given in Tables 2.1 and 2.2.

2.2.4 MIMO Channel

MIMO systems are equipped with multiple antennas at both transmitter and receiver. Let N_t and N_r be the number of transmit and receive antennas. The MIMO channel can be described using a $N_r \times N_t$ matrix:

$$\mathbf{H}(t,\tau) = \begin{bmatrix} h_{11}(t,\tau) & \dots & h_{1N_t}(t,\tau) \\ \vdots & \ddots & \vdots \\ h_{N_r1}(t,\tau) & \dots & h_{N_rN_t}(t,\tau) \end{bmatrix} \tag{2.33}$$

where $h_{ji}(t,\tau)$ is the time-varying impulse response between the ith transmit antenna and the jth receive antenna.

It is also possible to describe $h_{ji}(t,\tau)$ using the double-directional channel impulse model [45]:

$$h_{ji}(t,\tau) = \int\int\int h(\mathbf{r}_{Tx}^{(i)}, \mathbf{r}_{Rx}^{(j)}, t, \tau', \phi, \psi) G_{Tx}^{(i)}(\phi) G_{Rx}^{(j)}(\psi) f(\tau - \tau') d\tau' d\phi d\psi \tag{2.34}$$

where τ', ϕ and ψ denote, respectively, the excess delay, the direction of departure (DoD) and the direction of arrival (DoA), $\mathbf{r}_{Tx}^{(i)}$ and $\mathbf{r}_{Rx}^{(j)}$ are the coordinates of the ith transmit and jth receive antenna, and $h(\mathbf{r}_{Tx}^{(i)}, \mathbf{r}_{Rx}^{(j)}, t, \tau', \phi, \psi)$ is the double-directional channel impulse model and consists of the contributions of all individual multipath component. Furthermore, $G_{Tx}^{(i)}(\phi)$ and $G_{Rx}^{(j)}(\psi)$ represent, respectively, the transmit and receive antenna patterns and $f(\tau)$ is the overall impulse response.

Using the double-directional channel impulse model we have

$$h(\mathbf{r}_{Tx}^{(i)}, \mathbf{r}_{Rx}^{(j)}, t, \tau', \phi, \psi) = \sum_{l=0}^{N_p-1} h_l(\mathbf{r}_{Tx}^{(i)}, \mathbf{r}_{Rx}^{(j)}, t, \tau', \phi, \psi) \tag{2.35}$$

where N_p is the total number of multipath components. For planar waves, the contribution of the lth multipath component is given from the single-input single-output (SISO) case by

$$h_l(\mathbf{r}_{Tx}, \mathbf{r}_{Rx}, t, \tau, \phi, \psi) = \alpha_l e^{j\beta_l} \delta(\tau - \tau_l)\delta(\phi - \phi_l)\delta(\psi - \psi_l) \tag{2.36}$$

where α_l, β_l, τ_l, ϕ_l and ψ_l are, respectively, the amplitude, phase, delay, DoD and DoA associated with the lth multipath component. These parameters can also be time varying.

The input–output relation between the transmit signal vector $\mathbf{s}(t)$ and the received signal vector $\mathbf{y}(t)$ is given by

$$\mathbf{y}(t) = \int \mathbf{H}(t,\tau)\mathbf{s}(t-\tau)d\tau + \mathbf{n}(t) \tag{2.37}$$

where $\mathbf{n}(t)$ is the noise vector.

If the channel can be treated as approximately constant over the total frequency bandwidth (frequency flat channel) and over the observation time, the corresponding input–output relationship (2.37) simplifies to

$$\mathbf{y}(t) = \mathbf{H}\mathbf{s}(t) + \mathbf{n}(t) \tag{2.38}$$

where $\mathbf{H}$ is the $N_r \times N_t$ narrowband MIMO channel matrix given by

$$\mathbf{H} = \begin{bmatrix} h_{11} & \dots & h_{1N_t} \\ \vdots & \ddots & \vdots \\ h_{N_r 1} & \dots & h_{N_r N_t} \end{bmatrix} \tag{2.39}$$

2.2.4.1 MIMO Channel Model Classification

While we often assume that the elements of narrowband MIMO channel matrix are independent and identically distributed (i.i.d.), in reality, due to insufficient spacing between antenna elements and limited scattering in the environment, the fading is not independent. Therefore, the MIMO channel models should take this effect into account. The MIMO channel models can be divided into physical and nonphysical models.

Physical models choose some crucial physical parameters to describe the MIMO propagation channels. Some typical parameters include AoA, angle of departure (AoD), and time of arrival (TOA). However, under many propagation conditions, the MIMO channels are not well described by a small number of physical parameters and this makes it difficult, if not impossible, to identify the models. Although one attempts to separate the propagation channel from the measurement equipment (antenna responses, configuration, etc.) to allow extrapolation to other conditions, the model always contains some limitations related to the conditions under which the model was identified (point source assumption, etc.).

Physical models can be mainly split into deterministic models, geometry-based stochastic models, and nongeometric stochastic models:

- Deterministic channel models aim at reproducing the actual physical radio propagation process for a given environment. The characterization of the physical propagation parameters is performed in a completely deterministic manner like ray tracing and stored measurement data.
- In geometry-based stochastic channel models (GSCM), the impulse response is characterized by the laws of wave propagation applied to specific transmitter, receiver and scatterer geometries, which are chosen in a stochastic (random) manner.
- Nongeometric stochastic models describe and determine physical parameters (DoD, DoA, delay, etc.) in a completely stochastic way using underlying probability distribution functions without assuming an underlying geometry.

Nonphysical models characterize the impulse response or equivalently the transfer function of the channel between the individual transmit and receive antennas in an analytical way without explicitly accounting for wave propagation. The individual impulse responses are subsumed into the MIMO channel matrix. The main strengths of the nonphysical models is that they rely on a small set of parameters which fully characterize the communication scenario, namely the

power gain of the MIMO channel matrix, correlation matrices describing the correlation properties at the transmitter and receiver side and the associated Doppler spectrum of the channel paths. Nonphysical models can be further subdivided into propagation-motivated models and correlation-based models:

- Propagation-motivated models use propagation parameters. Examples are the finite scatterer model and the maximum entropy model.
- Correlation-based models characterize the MIMO channel matrix statistically in terms of the correlations between the matrix entries. Examples are the Kronecker model [21, 39], the virtual channel representation model [43] and the eigenbeam model [55].

2.2.4.2 Nongeometric Stochastic Physical Channel Model

Nongeometrical stochastic physical models describe paths from transmitter and receiver Rx by statistical parameters only, without reference to the geometry of a physical environment. The most popular model is the so-called extended Saleh–Valenzuela model [42, 54].

In [42] Saleh and Valenzuela have proposed a wideband SISO multipath channel model for the indoor scenario based on the indoor measurements. They proposed to model clusters of multipath components since they observed that the multipath components arrive in groups and therefore the scatterers could be separated into clusters. In the Saleh–Valenzuela model, the cluster amplitude is Rayleigh distributed with an exponential decaying profile. The multipath components within the individual clusters are zero-mean complex Gaussian also characterized by a second exponential profile with a steeper slope.

Suppose there are L_C clusters and each cluster has K_C rays, the directional channel response can be expressed as

$$h(\mathbf{r}_{Tx}, \mathbf{r}_{Rx}, t, \tau, \phi, \psi) = \frac{1}{\sqrt{L_C K_C}} \sum_{l=1}^{L_C} \sum_{k=1}^{K_C} \alpha_{kl} e^{j\beta_{kl}} \delta(\tau - \tau_{kl}) \delta(\phi - \phi_l - \phi_{kl}) \delta(\psi - \psi_l - \psi_{kl}) \tag{2.40}$$

where α_{kl}, β_{kl}, and τ_{kl} are the amplitude, phase, and delay of the kth ray in the lth cluster, ϕ_l and ψ_l are, respectively, the mean DoD and DoA associated with the lth cluster, and ϕ_{kl} and ψ_{kl} are the relative transmit and receive angles for the kth ray in the lth cluster.

Assuming that the AoA and AoD statistics are independent and identical, the Saleh–Valenzuela model was extended to MIMO channels in [54].

In the extended Saleh–Valenzuela model the probability density function of the ray AoA/AoD is Laplacian distributed:

$$p(\phi_{kl}) = \frac{1}{\sqrt{2}\sigma} \exp(-\sqrt{2}|\phi_{kl} - \phi_l|) \tag{2.41}$$

$$p(\psi_{kl}) = \frac{1}{\sqrt{2}\sigma} \exp(-\sqrt{2}|\psi_{kl} - \psi_l|) \tag{2.42}$$

2.2.4.3 Correlation-Based Model

Following the MIMO modeling approach presented in [20, 44] that utilizes receive and transmit correlation matrices, the MIMO channel matrix $\mathbf{H}$ can be separated into a fixed (constant, LOS) matrix and a Rayleigh (variable, NLOS) matrix:

$$\mathbf{H} = \sqrt{\frac{1}{1+K_R}}\mathbf{H}_s + \sqrt{\frac{K_R}{1+K_R}}\mathbf{H}_d \tag{2.43}$$

where K_R is the Rician K-factor. The matrix $\mathbf{H}_d$ is the fixed LOS matrix and the matrix $\mathbf{H}_s$ is the NLOS (Rayleigh) matrix. The elements of $\mathbf{H}_s$ are correlated zero-mean, complex Gaussian random variables.

For simplicity, in the rest of this section we will assume $K_R = 0$ that is $\mathbf{H} = \mathbf{H}_s$ (Rayleigh fading).

Let $\mathbf{h_{vec}}$ be the $N_t N_r \times 1$ vector obtained by vectorization of the channel matrix $\mathbf{H}$ as follows:

$$\begin{aligned} \mathbf{h_{vec}} &= [h_{11}\ h_{21}\ \ldots\ h_{N_t N_r}]^T \\ &= \text{vec}\{\mathbf{H}\} \end{aligned} \tag{2.44}$$

where vec$\{\mathbf{H}\}$ creates a column vector from the matrix $\mathbf{H}$. The zero-mean distribution multivariable complex Gaussian distribution of $\mathbf{h}_{vec}$ is given by

$$p(\mathbf{h_{vec}}) = \frac{1}{\det[\mathbf{R_H}]} \exp(-\mathbf{h_{vec}}^H \mathbf{R_H}^{-1} \mathbf{h_{vec}}) \tag{2.45}$$

where $\mathbf{R_H} = \mathbb{E}[\mathbf{h_{vec}}\mathbf{h_{vec}}^H]$ is the $N_t N_r \times N_t N_r$ semidefinite correlation matrix which describes the correlation between each pair of coefficient channels.

From (2.45), any channel realization is obtained by

$$\mathbf{h_{vec}} = \mathbf{R_H}^{1/2} \mathbf{g_{vec}} \tag{2.46}$$

where $\mathbf{g_{vec}}$ is a $N_t N_r \times 1$ vector of i.i.d unit variance elements.

2.2.4.4 Independent and Identically Distributed Model

The simplest analytical MIMO model is the independent and identically distributed (i.i.d.) model. The time varying multipath fading channel models can be used for each antenna pair from transmit antenna to receive antenna if MIMO channel coefficients are assumed to be i.i.d. This commonly used MIMO model is also called "rich scattering" model.

Since all elements of the MIMO channel matrix $\mathbf{H}$ are assumed uncorrelated we have

$$\mathbf{R}_{\mathbf{H}} = \mathbf{I} \tag{2.47}$$

This model is often used for theoretical considerations like the information-theoretic analysis of MIMO systems.

2.2.4.5 Kronecker Model

The so-called Kronecker model, where it is assumed that the spatial correlation matrix of the MIMO radio channel is separable, was proposed in [21, 39].

Let's define the transmit and the receive correlation matrices, respectively:

$$\mathbf{R}_{tx} = \frac{1}{N_R}\mathbb{E}\left[\mathbf{H}^H\mathbf{H}\right] \qquad \mathbf{R}_{rx} = \frac{1}{N_T}\mathbb{E}\left[\mathbf{H}\mathbf{H}^H\right] \tag{2.48}$$

These symmetrical complex correlation matrices can also be written as

$$\mathbf{R}_{tx} = \begin{bmatrix} \rho^t_{11} & \rho^t_{12} & \cdots & \rho^t_{1N_t} \\ \rho^t_{21} & \rho^t_{22} & \cdots & \rho^t_{2N_t} \\ \vdots & \ddots & \cdots & \vdots \\ \rho^t_{N_t1} & \rho^t_{N_t2} & \cdots & \rho^t_{N_tN_t} \end{bmatrix} \quad \text{and} \quad \mathbf{R}_{rx} = \begin{bmatrix} \rho^r_{11} & \rho^r_{12} & \cdots & \rho^r_{1N_r} \\ \rho^r_{21} & \rho^r_{22} & \cdots & \rho^r_{2N_r} \\ \vdots & \ddots & \cdots & \vdots \\ \rho^r_{N_r1} & \rho^r_{N_r2} & \cdots & \rho^r_{N_rN_r} \end{bmatrix}. \tag{2.49}$$

The complex spatial correlation coefficients at the transmitter side between antenna i_1 and i_2 and at the receiver side between antenna j_1 and j_2 considering the channel transfer matrix in (2.39) and assuming all antenna elements in the two arrays have the same polarization and the same radiation pattern, are given by

$$\rho^t_{i_1i_2} = < h_{i_1j}, h_{i_2j} > \quad \text{and} \quad \rho^r_{j_1j_2} = < h_{ij_1}, h_{ij_2} > \tag{2.50}$$

respectively, where $< u, v >$ computes the correlation coefficient between u and v.

$$< u, v > = \frac{\mathbb{E}[uv^*] - \mathbb{E}[u]\mathbb{E}[v^*]}{\sqrt{(\mathbb{E}[|u|^2] - |\mathbb{E}[u]|^2)(\mathbb{E}[|v|^2] - |\mathbb{E}[v]|^2)}} \tag{2.51}$$

Provided that $\rho^t_{i_1i_2}$ and $\rho^r_{j_1j_2}$ are independent of j and i, respectively. The spatial correlation matrix of the MIMO radio channel is the Kronecker product of the transmit and receive correlation matrices as follows:

$$\mathbf{R}_{\mathbf{H}} = \mathbf{R}^T_{tx} \otimes \mathbf{R}_{rx} \tag{2.52}$$

where $\otimes$ is the Kronecker product.[1]

From (2.46), the relation (2.52) simplifies to

$$\mathbf{h}_{\mathbf{vec}} = (\mathbf{R}_{tx}^{T} \otimes \mathbf{R}_{rx})^{1/2} \mathbf{g}_{\mathbf{vec}} \tag{2.53}$$

An alternative approach is given by

$$\mathbf{H} = \mathbf{R}_{rx}^{1/2} \mathbf{G} \mathbf{R}_{tx}^{1/2} \tag{2.54}$$

The matrix $\mathbf{G} = \text{unvec}\{\mathbf{g}_{\mathbf{vec}}\}$ is an i.i.d. unit variance MIMO channel matrix of size $N_R \times N_T$ and $\text{unvec}\{\mathbf{g}_{\mathbf{vec}}\}$ creates a matrix from the column vector $\mathbf{g}_{\mathbf{vec}}$ with the same number of elements.

For the case $N_t = N_r = 2$, the two Hermitian matrices $\mathbf{R}_{tx}$ and $\mathbf{R}_{rx}$ have the form

$$\mathbf{R}_{tx} = \begin{bmatrix} 1 & t^* \\ t & 1 \end{bmatrix} \qquad \mathbf{R}_{rx} = \begin{bmatrix} 1 & r^* \\ r & 1 \end{bmatrix} \tag{2.55}$$

where t and r are the transmit and received correlation. The 4×4 spatial correlation matrix is given by

$$\mathbf{R}_{\mathbf{H}} = \begin{bmatrix} 1 & r^* & t & s_1 \\ r & 1 & s_2 & t \\ t^* & s_2^* & 1 & r^* \\ s_1^* & t^* & r & 1 \end{bmatrix} \tag{2.56}$$

where $s_1 = \mathbb{E}[h_{1,1} h_{2,2}^*]$ and $s_2 = \mathbb{E}[h_{2,1} h_{1,2}^*]$ are the cross-channel correlations.

The Kronecker model is one of the most often-used channel model to model the second-order statistics of the channel. However, this separable model is not always accurate and discrepancies have been reported in measurement campaigns when the number of antennas is high [37]. To allow arbitrary coming between the transmit and receive parts, the virtual channel representation model has been proposed in [43]. The author utilizes a fixed and predefined virtual partitioning of the spatial domain to characterize the MIMO channel.

A more accurate model is the eigenbeam or Weichselberger model [55] that combines the advantages of both the Kronecker model and the virtual channel representation. The eigenbeam model treats the influence of the antennas and

[1] If $\mathbf{A}$ is a $M \times N$ matrix with elements a_{mn} and $\mathbf{B}$ is a matrix, the Kronecker product $\mathbf{A} \otimes \mathbf{B}$ is

$$\mathbf{A} \otimes \mathbf{B} = \begin{bmatrix} a_{11}\mathbf{B} & \dots & a_{1N}\mathbf{B} \\ \vdots & \ddots & \vdots \\ a_{M1}\mathbf{B} & \dots & a_{MN}\mathbf{B} \end{bmatrix}.$$

environment by means of eigenbases and a coupling matrix. Let $\mathbf{U}_{rx}$ and $\mathbf{U}_{tx}$ be the eigenbases of the unparameterized one-sided correlation matrices of sides A and B of the link (correlation as perceived from the other side of the link). A MIMO channel realization is generated as

$$\mathbf{H} = \mathbf{U}_{rx}(\Omega \odot \mathbf{H}_W)\mathbf{U}_{tx}^T \tag{2.57}$$

where $\odot$ is the Hadamard (entry wise) product and $\mathbf{H}_W$ is a matrix of i.i.d. random zero-mean complex-normal distributed values. The elements of the coupling matrix Ω specify the mean amount of energy that is coupled from the mth eigenvector of side Rx to the nth eigenvector of side Tx.

The spatial correlation function is the Fourier transform of the power azimuth spectrum (PAS). For MIMO channel model with uniform linear array (ULA) and with the omnidirectional antenna spacing, the PAS distribution in physical channels can be considered as uniform, Gaussian and Laplacian. Using these three distributions, the envelope of correlation coefficient is computed as a function of the relative antenna spacing at the receiver Δ_r and at the transmitter Δ_t, AoA and AS by considering multicluster model.

For ULA, the complex correlation coefficients for the receive antennas apart form Δ_r are expressed as [44]

$$\rho^r(\Delta_r) = R^r_{xx}(\Delta_r) + jR^r_{xy}(\Delta_r), \tag{2.58}$$

where $\Delta_r = d_r/\lambda$ and d_r stands for the distance between the receive antennas and $\lambda = c/f_c$ is the wavelength of a narrowband signal with center frequency f_c. R^r_{xx} and R^r_{xy} are, respectively, the correlation functions between the real parts and between the real and imaginary parts

$$R^r_{xx} = \int_{-\pi}^{\pi} \cos(2\pi\Delta_r \sin\phi_r)\mathrm{PAS}(\phi_r)d\phi_r \quad \text{and} \quad R^r_{xy} = \int_{-\pi}^{\pi} \sin(2\pi\Delta_r \sin\phi_r)\mathrm{PAS}(\phi_r)d\phi_r, \tag{2.59}$$

where ϕ_r is the AoA for the receiver. The Laplacian PAS distribution which gives better match than Gaussian or uniform distributions for typical rural environment can be expressed as

$$\mathrm{PAS}(\phi_r) = \frac{1}{\sqrt{2}\sigma_r} \exp\left(-|\sqrt{2}\phi_r/\sigma_r|\right) \tag{2.60}$$

where σ_r is the standard deviation of PAS (which corresponds to the numerical rms value of AS). The same derivations can also be used to obtain correlation coefficients for the transmit antennas. For multipath fading channels, the derivation of correlation matrices is applied for each path individually.

When assuming that the AoD at the transmitter and AoA at the receiver are Gaussian distributed, respectively, around the mean AoD and AoA, i.e $\phi_r = \bar{\phi_r} + \hat{\phi_r}$

where $\hat{\phi}_r = N(0, \sigma_r^2)$ and $\phi_t = \bar{\phi}_t + \hat{\phi}_t$ where $\hat{\phi}_t = N(0, \sigma_t^2)$, it has been shown in [5] that for small angle spread, the spatial correlation coefficient using an ULA can be simplified as follows:

$$\rho^t_{i_1 i_2} = \exp(-j2\pi(i_1 - i_2)\Delta_t \cos(\bar{\phi}_t)) \exp(-0.5(2\pi(i_1 - i_2)\Delta_t \sin(\bar{\phi}_t)\sigma_t)^2) \quad (2.61)$$

$$\rho^r_{j_1 j_2} = \exp(-j2\pi(j_1 - j_2)\Delta_r \cos(\bar{\phi}_r)) \exp(-0.5(2\pi(j_1 - j_2)\Delta_r \sin(\bar{\phi}_r)\sigma_r)^2) \quad (2.62)$$

This model can be further simplified when the standard deviation of PAS $\sigma_t = 0$ and $\sigma_r = 0$. In this case, we have

$$\rho^t_{i_1 i_2} = \exp(-j2\pi(i_1 - i_2)\Delta_t \cos(\bar{\phi}_t)) \quad (2.63)$$

$$\rho^r_{j_1 j_2} = \exp(-j2\pi(j_1 - j_2)\Delta_r \cos(\bar{\phi}_r)) \quad (2.64)$$

2.2.5 *Dual-Polarized Antennas*

Since the vertical and horizontal polarizations are sufficient to characterize the far field, polarization can be taken into account by extending the impulse response to a polarimetric 2×2 matrix.

Handsets and small devices may not have adequate space for more than two elements linear array. For this reason, the use of dual-polarized antennas is a promising cost- and space-effective alternative, where two spatially separated uni-polarized antennas are replaced by a single antenna structure employing two orthogonal polarizations. The main advantage of exploiting polarization diversity is that the large antenna configurations of space diversity are not necessary to achieve performance gain.

As early as 1990, experimenters such as Rodney Vaughan [53] have tested the concept of polarization-diversity systems:

For suburban base stations, the dominance of the vertical polarization makes the diversity gain rather small—only a couple of decibels at the 99.5% probability level,

In urban environments, however, the diversity gain is nearly 7 dB at the 99.5% level, offering much promise for system design using polarization diversity.

Polarization diversity is created by the nature of the wireless communication system that the signal energy from one polarization is generally coupled into other polarizations. Indeed, multiple reflections between the transmitter and the receiver lead to depolarization of radio waves, coupling some energy of the transmitted signal into the other polarized wave [22, 24, 53].

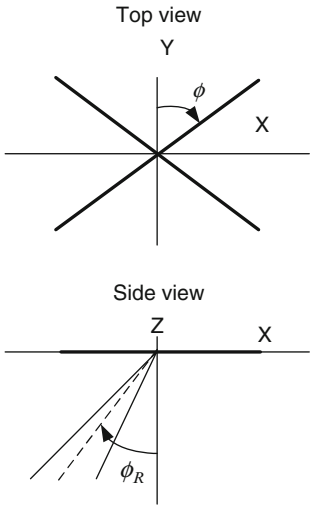

Fig. 2.7 Cross-polarized antenna

Due to nonideal antennas cross-polar isolation (XPI) and the existence of cross-polar ratio (XPR) in the multipath radio channel, vertically/horizontally polarized transmitted waves have also horizontal/vertical component. When we combine both effects, we obtain the cross-polar discrimination (XPD).

Depolarization caused by nonideal antennas is well known in antenna theory and related to the cross-polar antenna pattern. This can be modelized by a coupling matrix

$$\mathbf{X}_a = \begin{bmatrix} 1 & \sqrt{\chi_a} \\ \sqrt{\chi_a} & 1 \end{bmatrix} \tag{2.65}$$

where χ_a^{-1} is the scalar antenna XPI. For an ideal antenna, we have $\chi_a = 0$.

In the rest of this chapter, we will assume that the co-located antenna have a high XPI and that consequently, we can do the approximation $XPD \approx XPR$. We now consider a downlink communication link with one dual-polarized antenna at both the transmitter and the receiver side with vertical (V_{pol}) and horizontal (H_{pol}) polarization states.

In Fig. 2.7, we show a cross-polarized antenna where a narrow AoA spread is received from an average AoA $\bar{\phi}_r$. The AoA is considered to have an angle spread as given by a probability density function, $p(\phi_r)$.

The system model can be described by the matrix relation $\mathbf{r} = \mathbf{G}\mathbf{x} + \mathbf{n}$, where $\mathbf{x}$ is the 2×1 transmit signal vector and $\mathbf{r}$ is the 2×1 received vector. $\mathbf{G}$ is the 2×2 channel or polarization matrix involving complex Gaussian random variables:

$$\mathbf{G} = \begin{bmatrix} g_{vv} & g_{vh} \\ g_{hv} & g_{hh} \end{bmatrix} \tag{2.66}$$

where g_{hh}, g_{vh}, g_{hv} and g_{vv} represent the complex channel gain coefficients for transmission between horizontal receive and horizontal transmit, vertical and horizontal, horizontal and vertical and vertical and vertical antennas, respectively.

Let's denote $p_{ij} = |g_{ij}|^2$. Different cross-polar ratios can be defined [36]:

Uplink cross-polar ratios

$$XPR_{U^v} = p_{vv}/p_{vh} \qquad XPR_{U^h} = p_{hh}/p_{hv} \tag{2.67}$$

Downlink cross-polar ratios

$$XPR_{D^v} = p_{vv}/p_{hv} \qquad XPR_{D^h} = p_{hh}/p_{vh} \tag{2.68}$$

Co-polar ratio (CPR)

$$CPR_{D^v} = p_{vv}/p_{hh} \tag{2.69}$$

Experimental data collected reveal that the elements of the polarization matrix $\mathbf{G}$ are correlated. We can define the correlation matrix given by $\mathbb{E}[\text{vec}\{\mathbf{G}\}\text{vec}\{\mathbf{G}^H\}]$. The diagonal elements are, respectively, the average gain $\mathbb{E}[p_{vv}]$, $\mathbb{E}[p_{hv}]$, $\mathbb{E}[p_{vh}]$ and $\mathbb{E}[p_{hh}]$. The cross-polar correlations (XPC) are, respectively, the transmit and receive correlation coefficients

$$\rho^t =< g_{hh}, g_{hv} >=< g_{vh}, g_{vv} > \tag{2.70}$$

$$\rho^r =< g_{hh}, g_{vh} >=< g_{hv}, g_{vv} > \tag{2.71}$$

The correlation between g_{hh} and g_{vv} is defined as the co-polar correlation (CPC) while the correlation between g_{vh} and g_{hv} is the anti-polar correlation (APC) [36].

A theoretical model for characterizing correlation between diversity branches in a polarization diversity system was first established by Kozono et al. [22] assuming a narrowband multipath beam arriving from the azimuth. Vaughan [53] further extends Kozono's model to take into account the rotation of two antennas with a fixed angular separation around their phase center. When the angle spread probability distribution is a Laplacian distribution as given in (2.60), the correlation coefficient can be computed from [22, 33] as follows:

$$\rho(\phi_{ant}, \phi_r, XPR) = \left[\frac{-\tan^2(\phi_{ant})\mathbb{E}[\cos^2(\phi_r)] + XPR}{\tan^2(\phi_{ant})\mathbb{E}[\cos^2(\phi_r)] + XPR}\right] \tag{2.72}$$

where $\mathbb{E}[\cos^2(\phi_r)]$ is the expected value calculated from the probability density function $p(\phi_r)$.

Figure 2.8 shows the correlation in function of the mean AoA. It is obtained using (2.72) by transmitting a vertically polarized signal which suffers depolarizing effects in the environment and received with the cross-polarized subscriber antennas

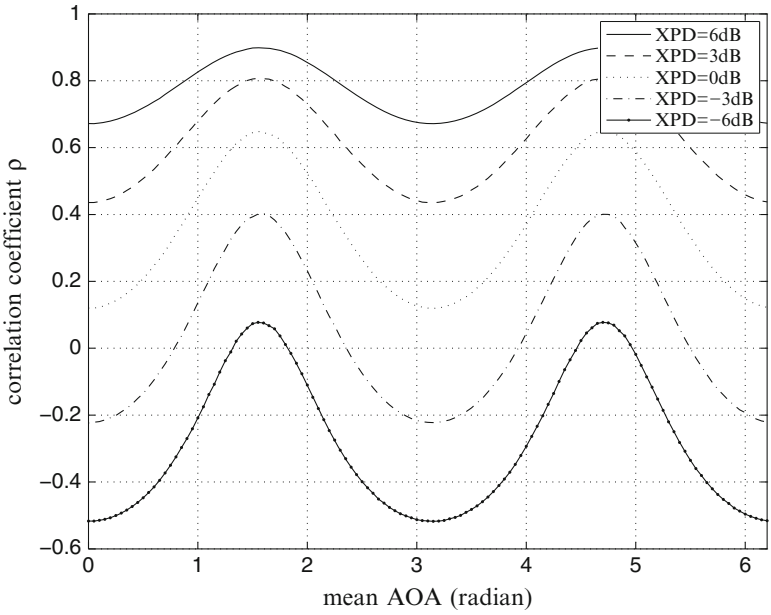

Fig. 2.8 Correlation versus XPR for dual-polarized $\phi = \pm 45°$ antennas, Laplacian PAS = 35°

for dual-polarized $\phi = \pm 45°$ antennas and an angle spread of 35° (Laplacian distribution).

We can see that the effect of the antenna orientation produces a significant change in the correlation between the branches. For example, when XPR = 6 dB, the correlation coefficient is quite high (> 0.65) for all mean AoA. While these results give some hints on the link between XPR and correlation coefficient, it is also important to evaluate the distribution of the power ratio XPR for each considered scenario as we will see later.

Correlation between orthogonal components of the electromagnetic field at the mobile has been extended in [6,46] to a uniform but arbitrarily wide angular spread.

Different experimental results have been conducted and published for both outdoor and indoor scenario in the last decade. We can summarize the main properties of dual-polarized channels as follows:

- The typical values of average CPR vary between 4 and 5.5 dB in urban microcell and between 3 and 11 dB in suburban microcell [30].
- The typical values of average XPR vary in the urban/suburban environment between 3 and 9 dB, with an average of 6 dB. In a rural environment, the average XPR is between 10 and 18 dB, due to the pure LOS connection and the absence of obstacles that couple the signal from the V_{pol} into the H_{pol}. The same results are observed in indoor [22,23,28–30,53].

- Experimental results have also shown that the cross-polar correlation between the V_{pol} and the H_{pol} at the receiver is generally less than 0.2 [19, 28, 30].

2.2.5.1 Dual-Polarized Rayleigh Fading Channels

In Rayleigh fading, it has been shown that spatial correlation can be considered independent of the polarization if the antennas have the same directional spectrum. Under this assumption, the dual-polarized channel matrix denoted as $\mathbf{H}_x$ can be modelized, thanks to the separation of space and polarization effects as follows [36]:

$$\mathbf{H}_x = \mathbf{H} \odot \mathbf{X} \tag{2.73}$$

where $\mathbf{H}$ is the uni-polarized correlated Rayleigh channel matrix and $\mathbf{X}$ models the correlation and power imbalance of the channel depolarization. The relation between $\mathbf{X}$ and $\mathbf{G}$ is

$$\mathbf{G} = h\mathbf{X} \tag{2.74}$$

where h is a scalar complex Gaussian term representing the fading. A general model of $\mathbf{X}$ for VH to VH downlink transmission can be given by

$$\text{vec}\{\mathbf{X}\} = \begin{bmatrix} 1 & \sqrt{\mu\chi}\vartheta & \sqrt{\chi}\sigma & \sqrt{\mu}\delta_1 \\ \sqrt{\mu\chi}\vartheta^* & \mu\chi & \sqrt{\mu}\chi\delta_2 & \mu\sqrt{\chi}\sigma \\ \sqrt{\chi}\sigma^* & \sqrt{\mu}\chi\delta_2^* & \chi & \sqrt{\mu\chi}\vartheta \\ \sqrt{\mu}\delta_1^* & \mu\sqrt{\chi}\sigma^* & \sqrt{\mu\chi}\vartheta^* & \mu \end{bmatrix}^{1/2} \text{vec}\{\mathbf{X}_W\} \tag{2.75}$$

where

- μ and χ are, respectively, the CPR and downlink XPR.
- σ is the receive correlation coefficient (between VV and VH, HV and HH).
- ϑ is the transmit correlation coefficient (between VV and HV, VH and HH).
- δ_1 is the CPC coefficient (between VV and HH).
- δ_2 is the APC coefficient (between HV and VH).
- The elements of the 2×2 matrix $\mathbf{X}_W$ have unit amplitude and angles, ϕ_n $n = 1, \ldots, 4$ uniformly distributed over $[0, 2\pi]$.

2.2.5.2 Dual-Polarized MIMO Fading Channels

When the Tx and Rx array are made of $N_t/2$ and $N_r/2$ dual-polarized arrays, the Rayleigh channel matrix can be written as

$$\mathbf{H}_{x,N_r \times N_t} = \mathbf{H}_{N_r/2 \times N_t/2} \odot \mathbf{X} \tag{2.76}$$

In [34] the authors have investigated the performance of spatial multiplexing and Alamouti scheme in MIMO wireless systems employing dual-polarized antennas. They have shown that while improvements in terms of symbol error rate of up to an order of magnitude are possible in the case of spatial multiplexing, the presence of polarization diversity generally incurs a performance loss compared to spatial diversity for transmit diversity techniques such as Alamouti scheme.

2.3 Orthogonal Frequency Division Multiplexing

Different techniques can cope with the intersymbol interference due to frequency selective channel. Among these techniques, multicarrier modulations avoid the use of complex equalizer at the receiver side. In multicarrier modulation, the data stream is divided into multiple substreams to be transmitted over different orthogonal subchannels centered at different subcarrier frequencies. Consider a linearly modulated system with data rate R and passband bandwidth B_W. The coherence bandwidth for the channel is assumed to be $B_{coh} < B_W$, so the signal experiences frequency-selective fading. The basic idea of multicarrier modulation is to break this wideband system into N linearly modulated subsystems in parallel, each with subchannel bandwidth $B_N = B_W/N$. The number of subchannels N is chosen to make the symbol time on each substream much greater than the delay spread of the channel in order to eliminate intersymbol interference. In the frequency domain this is equivalent to making the substream bandwidth less than the channel coherence bandwidth. For N being sufficiently large, the subchannel bandwidth $B_N << B_{coh}$, which insures relatively flat fading on each subchannel. This can also be seen in the time domain: the symbol time T_N of the modulated signal in each subchannel is equal to $\frac{1}{B_N}(1+\epsilon)$. ϵ/T_N is the additional bandwidth due to the time limiting of the filter responses. So it implies that $T_N = \frac{1}{B_N}(1+\epsilon) >> 1/Bc \approx T_m$, where T_m denotes the delay spread of the channel. So each subchannel experiences little ISI. Figure 2.9 illustrates the multicarrier modulation without overlapping subcarriers.

We can improve the spectral efficiency of multicarrier modulation by overlapping the subchannels. The subcarriers must still be orthogonal so that they can be separated out by the demodulator at the receiver. The subcarriers $\cos(2\pi(f_0 + n/T_N)), n = 0, 1, \ldots, N-1$ form a set of approximately orthogonal basis functions on the interval $[0, T_N]$. Figure 2.10 illustrates the multicarrier modulation with overlapping subcarriers.

Multicarrier modulation can be efficiently implemented digitally using the discrete Fourier transform (DFT) and the inverse DFT (IDFT). Using this discrete implementation, called OFDM, the ISI can be completely eliminated through the use of a cyclic prefix [27].

The main idea of OFDM transmission is to turn the channel convolutional effect into a multiplicative one. In order to perform this transformation, it can be noticed

that a circular convolution is a multiplication in the frequency domain. Unfortunately, the channel output is not a circular convolution but a linear convolution. However, the linear convolution between the channel input and its impulse response can be turned into a circular convolution by adding a special prefix to the input called a cyclic prefix.

From the sequence $\mathbf{X}[m]$ by applying the IDFT, we obtain

$$x_{i,m} = \frac{1}{\sqrt{N}} \sum_{n=0}^{N-1} X_{n,m} \exp\left(\frac{2j\pi ni}{N}\right) \tag{2.77}$$

In the continuous time domain, we have

$$x_m(t) = \frac{1}{\sqrt{N}} \sum_{n=0}^{N-1} X_{n,m} \exp\left(2j\pi f_n t\right) g(t) \tag{2.78}$$

where $g(t)$ is the pulse shaping. The transmitted signal is

$$x(t) = \sum_m \frac{1}{\sqrt{N}} \sum_{n=0}^{N-1} X_{n,m} \exp\left(2j\pi f_n t\right) g(t - mT) \tag{2.79}$$

where T is the OFDM symbol period. Figure 2.11 gives a description of the OFDM implementation.

The input data are modulated using a QAM or M-PSK modulator resulting in a complex symbol stream $\mathbf{X}[m] = [X_{0,m} X_{1,m} \ldots X_{N-1,m}]$. Each symbol is transmitted over one subcarrier. Thus, the N output symbols from the serial-to-parallel converter are the discrete frequency components of the OFDM modulator output $x(t)$. In order to generate x(t), these frequency components are converted into time samples by performing an IDFT on these N symbols, which is efficiently implemented using the IFFT algorithm. The IFFT yields the OFDM symbol consisting of the sequence

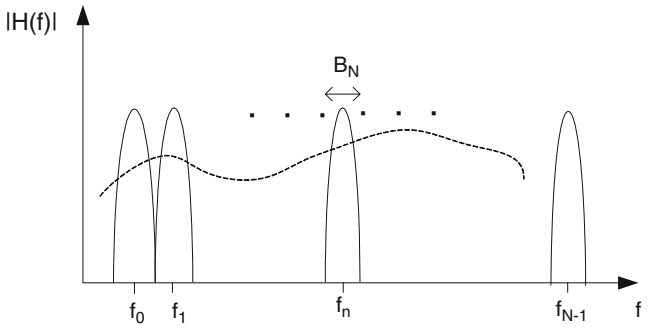

Fig. 2.9 A multicarrier without overlapping subcarriers

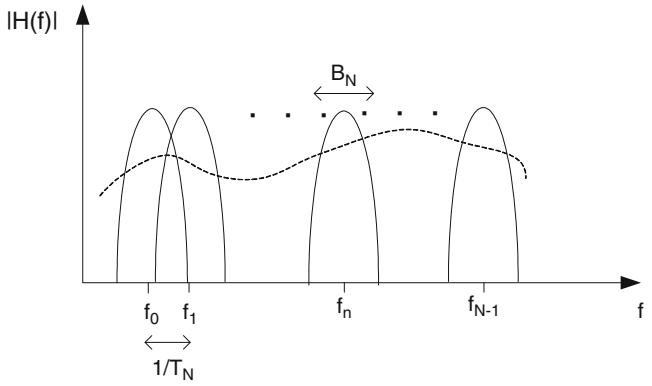

Fig. 2.10 A multicarrier with overlapping subcarriers

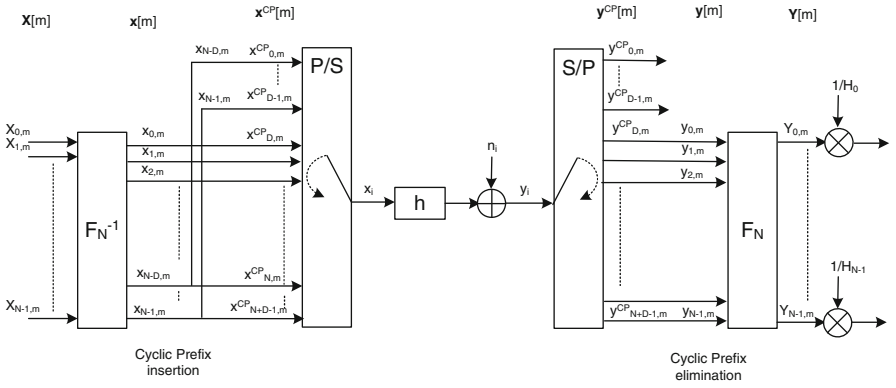

Fig. 2.11 OFDM implementation

$\mathbf{x}[m] = [x_{0,m} x_{1,m} \ldots x_{N-1,m}]$ of length N:

$$\mathbf{x}[m] = \mathbf{F}_N^{-1} \mathbf{X}[m] \tag{2.80}$$

$\mathbf{F}_N^{-1} = \mathbf{F}_N^H$ is the inverse of the Fourier matrix $\mathbf{F}_N$.

At the output of the IFFT, a cyclic prefix (CP) or guard interval of D samples is added at the beginning of each block and the resulting vector is $\mathbf{x}^{CP}[m] = [x_{N-D,m}, \ldots, x_{N-1,m}, x_{1,m}, \ldots, x_{i,m}, \ldots x_{N-1,m}]$. The length D should be longer than the time spread L of the channel ($D > L$). Since the redundancy is $\dfrac{N}{N+D}$, N should be much higher than D in order to limit the negative impact of the prefix cyclic on the efficiency of the scheme. After a parallel to serial conversion (P/S) the sequence is passed through a digital to analog converter (DAC).

The time invariant selective additive white Gaussian noise (AWGN) channel can be described using its equivalent discrete baseband impulse response

$$\mathbf{h}[m] = [h_{0,m}, \ldots, h_{L-1,m}, 0, \ldots, 0] \tag{2.81}$$

At the receiver after analog to digital conversion, the received signal is given by

$$y_{i,m} = \sum_{l=0}^{L-1} h_{l,m} x_{i-l,m} + n_{i,m} \tag{2.82}$$

We assume that the channel response does not change during the OFDM symbol duration. The frequency response of the channel is the Fourier transform of $\mathbf{h}[m]$: $\mathbf{H}[m] = \mathbf{F}_N^{-1}\mathbf{h}[m]$

At the receiver after analog to digital conversion the received signal is given by

$$\begin{aligned}\mathbf{y}^{CP}[m] = \begin{bmatrix} y_{0,m}^{CP} \\ y_{1,m}^{CP} \\ \vdots \\ \\ \vdots \\ \\ \vdots \\ y_{N+D-1,m}^{CP} \end{bmatrix}_{(N+D)\times 1} &= \mathbf{h}^{ISI}[m] \begin{bmatrix} x_{N-D,m} \\ \vdots \\ x_{N-1,m} \\ x_{0,m} \\ \vdots \\ x_{N-1,m} \end{bmatrix}_{(N+D)\times 1} \\ + \mathbf{h}^{IBI}[m] \begin{bmatrix} x_{N-D,m-1} \\ \vdots \\ x_{N-1,m-1} \\ x_{0,m-1} \\ \vdots \\ x_{N-1,m-1} \end{bmatrix}_{(N+D)\times 1} &+ \mathbf{n}[m]\end{aligned} \tag{2.83}$$

with

$$\mathbf{h}^{ISI}[m] = \begin{bmatrix} h_{0,m} & 0 & \ldots & \ldots & \ldots & 0 \\ \vdots & \ddots & \ddots & & & \vdots \\ h_{L,m} & & \ddots & \ddots & & \vdots \\ 0 & \ddots & & \ddots & \ddots & \vdots \\ \vdots & \ddots & \ddots & & \ddots & \vdots \\ 0 & \ldots & 0 & h_{L,m} & \ldots & h_{0,m} \end{bmatrix}_{(N+D)\times(N+D)}$$

$$\mathbf{h}^{IBI}[m] = \begin{bmatrix} 0 \ldots 0 & h_{L,m} \ldots & h_{1,m} \\ \vdots \ddots & \ddots \ddots & \vdots \\ \vdots \quad \ddots & \quad \ddots & h_{L,m} \\ \vdots \quad\quad \ddots & \quad\quad & 0 \\ \vdots \quad\quad\quad & \ddots & \vdots \\ 0 \ldots\ldots & \ldots \ldots & 0 \end{bmatrix}_{(N+D)\times(N+D)}$$

$\mathbf{h}^{ISI}[m]$ is the ISI due to the selectivity of the channel on the mth OFDM symbol and $\mathbf{h}^{IBI}[m]$ is the inter-block interference between the mth and $(m-1)$th OFDM symbols.

After removing the prefix cyclic corresponding to the D first samples, we obtain

$$\begin{bmatrix} y_{0,m} \\ \vdots \\ \vdots \\ \vdots \\ y_{N-1,m} \end{bmatrix}_{N\times 1} = \begin{bmatrix} h_{0,m} & 0 & \ldots & h_{L,m} & \ldots & h_{1,m} \\ \vdots & \ddots & \ddots & & \ddots & \vdots \\ h_{L,m} & & \ddots & \ddots & & h_{L,m} \\ 0 & \ddots & & \ddots & \ddots & \vdots \\ \vdots & \ddots & \ddots & & \ddots & 0 \\ 0 & \ldots & 0 & h_{L,m} & \ldots & h_{0,m} \end{bmatrix}_{N\times N} F_N^H \begin{bmatrix} X_{0,m} \\ \vdots \\ \vdots \\ \vdots \\ X_{N-1,m} \end{bmatrix}_{N\times 1} + \mathbf{n}[m] \tag{2.84}$$

Using the prefix cyclic we have been able to transform the linear convolution into a circular convolution. Since the circular convolution is equivalent to a multiplication in the frequency domain, the vector $\mathbf{X}_m$ has been transmitted over N parallel flat fading channel defined by a complex attenuation $H_{i,m}$.

$$\begin{bmatrix} Y_{0,m} \\ \vdots \\ \vdots \\ \vdots \\ Y_{N-1,m} \end{bmatrix}_{N\times 1} = \begin{bmatrix} H_{0,m} & 0 & \ldots\ldots\ldots & 0 \\ 0 & H_{1,m} & 0 \ldots\ldots & \ldots \\ \vdots & 0 & \ddots\ 0 \ldots & \ldots \\ \vdots & \ldots & \ldots \ddots \ldots & \ldots \\ \vdots & \ldots & \ldots\ldots \ddots & 0 \\ 0 & \ldots & \ldots\ldots\ 0 & H_{N-1,m} \end{bmatrix}_{N\times N} \begin{bmatrix} X_{0,m} \\ \vdots \\ \vdots \\ \vdots \\ X_{N-1,m} \end{bmatrix}_{N\times 1} + \mathbf{N}[m] \tag{2.85}$$

This input–output relation can be written as

$$\mathbf{Y}[m] = \text{diag}(\mathbf{H}[m])\mathbf{X}[m] + \mathbf{N}[m] \tag{2.86}$$

where $\text{diag}(\mathbf{H}[m])$ is a diagonal matrix of size $N \times N$ in which the entries outside the main diagonal are all zero and the diagonal entries are composed of the elements of the vector $\mathbf{H}[m]$.

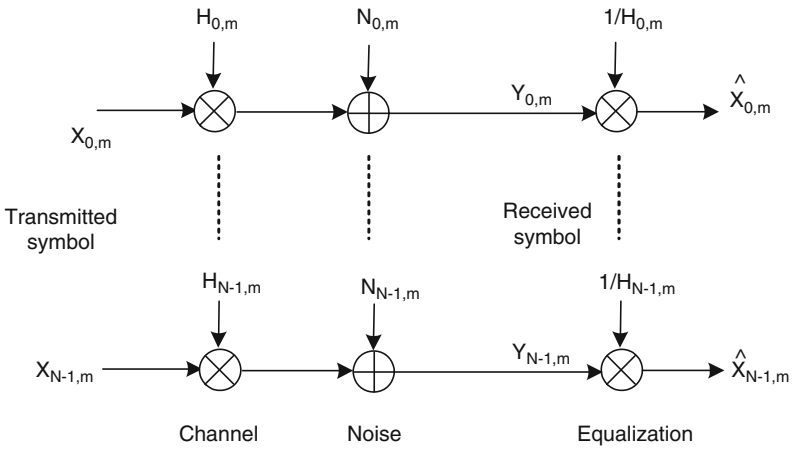

Fig. 2.12 Frequency model of OFDM scheme

Figure 2.12 gives the equivalent model of an OFDM transmission.

If the transmit power on subcarrier n is P_n and the fading on that subcarrier is H_n, then the received signal to noise ratio γ_n is

$$\gamma_n = |H_n|^2 P_n/(N_0 B_N) \tag{2.87}$$

where N_0 is the noise power spectral density.

If $|H_n|^2$ is small then the received SNR on the nth subchannel is quite low, which can lead to a high BER on that subchannel. Since flat fading can seriously degrade performance in each subchannel, it is important to compensate for flat fading in the subchannels.

Since OFDM does not exploit the frequency diversity, it is important to associate to this scheme interleaving and error correcting codes (convolutional codes, block codes, multidimensional constellations, turbo codes) to cope with fading.

2.4 MIMO Systems

2.4.1 Introduction

The next generation wireless communication systems are expected to provide users with mobile multimedia services such as high speed mobile internet access and mobile computing. In order to meet this rapidly growing demand at better quality of services at higher data rates and higher mobility, innovative techniques that improve link reliability and spectral efficiency are needed in mobile propagation environment.

In conventional single transmit and single receive antenna system or SISO system, increasing the data rate can be achieved by increasing either the transmission bandwidth which is expensive and restricted in many cases or the transmission power that requires an expensive amplifier and causes to reduce the battery life of mobile units.

The development of MIMO communication systems that use multiple transmit and multiple receive antennas provides the ability to design spectrally efficient systems without extra power and bandwidth. Assuming that the channels between the transmit and received antennas are independent, Foshini [12] and Telatar [49] have shown that the channel capacity grows linearly with $\min(N_t, N_r)$where N_t is the number of transmit antennas and N_r is the number of received antennas. This motivates to consider MIMO systems for transmission of high data rates in future wireless communication systems.

MIMO communication systems have two major advantages over SISO systems in wireless channels:

- Multiplexing gain: spatial multiplexing using layered space-time coding techniques (transmission of independent data over different antennas) enables to communicate at higher data rates without increasing the bandwidth or the transmit power.
- Spatial diversity: space-time codes (STC) [35] exploit the spatial diversity (both transmit and receive) available in the multiple spatial channels and improve the performance against fading channels while maintaining a good spectral efficiency. Such techniques include delay diversity, STBC [2,48] and space-time trellis code (STTC) [47].

A considerable amount of research has addressed the design and implementation of STC and spatial multiplexing systems for wireless flat fading channels. However, many communication channels are frequency selective in nature, for which the STC design problem becomes complicated. On the other hand, the OFDM technique which transforms a frequency selective channel into parallel flat fading subchannels is a potential candidate for high data rate wireless transmission. Hence, the combination of MIMO signal processing with OFDM is regarded as a promising solution for providing diversity and enhancing the data rates of next generation wireless communication systems operating over frequency selective fading channels. STC can be combined with OFDM in the time domain using coded STTC-OFDM [1,31] or coded STBC-OFDM systems [16,26] and in the frequency domain using space-frequency block coded (SFBC) OFDM systems [4,25].

The MIMO systems should be concatenated with outer channel codes in order to achieve near-capacity performance in wireless flat fading channels. Moreover, in multipath MIMO channels, the maximum achievable diversity order is also related to the number of propagation paths which is named as frequency diversity [5]. Since SFBC-OFDM and STBC-OFDM fail to exploit frequency diversity, concatenating them with an outer channel code and interleaver can provide more diversity compared to flat fading channels.

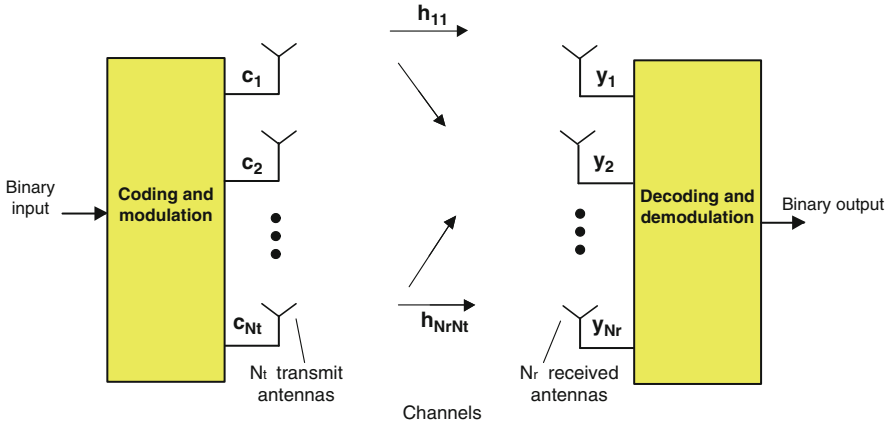

Fig. 2.13 The MIMO wireless transmission system

In this section, we shall present the necessary theories of MIMO systems in adequate depth. We will examine the principles and design criteria of the MIMO system in wireless channels by defining the potential gains. Then, we will present the well-known MIMO codes in detail such as spatial multiplexing code vertical-BLAST (V-BLAST), the orthogonal and non-orthogonal STBC. For these MIMO systems, we will only consider that the channel state information (CSI) is unknown at the transmitter and perfectly known at the receiver.

2.4.2 *Capacity of MIMO Systems*

We consider a MIMO communication link with N_t transmit antennas and N_r receive antennas, as illustrated in Fig. 2.13.

Assuming that the channel is flat fading, the signal from receive antenna j is a noisy superposition of transmitted signals from N_t transmit antennas as

$$y_j = \sum_{i=1}^{N_t} h_{ji} c_i + n_j, \tag{2.88}$$

where h_{ji} is the complex channel coefficient from transmit antenna i to receive antenna j and n_j is the additive noise which is modeled as independent samples of a zero-mean complex Gaussian random variable. There is a total power constraint, P on the signals from the transmit antennas. The noise power per receive antenna is $N_0 B$ where $N_0/2$ is the noise power spectral density and B is the bandwidth.

We define the channel coefficient matrix $\mathbf{H}$ with the dimension of $N_r \times N_t$ as follows:

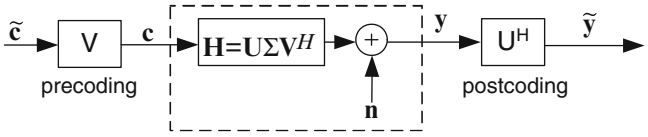

Fig. 2.14 SVD decomposition of the MIMO channel

$$\mathbf{H} = \begin{bmatrix} h_{11} & \dots & h_{1N_t} \\ \vdots & \ddots & \vdots \\ h_{N_r 1} & \dots & h_{N_r N_t} \end{bmatrix}. \tag{2.89}$$

Then, the received signal in (2.88) can be written in a matrix form as

$$\mathbf{y} = \mathbf{H}\mathbf{c} + \mathbf{n}, \tag{2.90}$$

where $\mathbf{y}$ and $\mathbf{n}$ are the received and noise matrices, respectively, with the dimension of $N_r \times 1$.

We decompose the MIMO channel matrix $\mathbf{H}$ into equivalent parallel SISO channels by using singular value decomposition (SVD) as (Fig. 2.14)

$$\mathbf{H} = \mathbf{U}\Sigma\mathbf{V}^H, \tag{2.91}$$

where $\mathbf{U} = [\mathbf{u}_1 \dots \mathbf{u}_{N_r}]$ of size $N_r \times N_r$ and $\mathbf{V} = [\mathbf{v}_1 \dots \mathbf{v}_{N_t}]$ of size $N_t \times N_t$ are unitary matrices, $\mathbf{u}_i$ and $\mathbf{v}_j$ are, respectively, the ith left singular and the jth right singular vector of the channel matrix $\mathbf{H}$. Σ is a rectangular matrix $\Sigma = \text{diag}(\sqrt{\lambda_1}, \sqrt{\lambda_2}, \dots, \sqrt{\lambda_r}, 0, \dots, 0)$ where $\lambda_1 \geq \lambda_2 \geq \dots \lambda_r$ are the nonzero eigenvalues of $\mathbf{H}^H\mathbf{H}$ (assuming $N_t \leq N_r$). The number of eigenvalues r equals to the rank of the channel matrix $\mathbf{H}$ which corresponds to $\min(N_t, N_r)$.

By applying preprocessing to the transmitted symbols ($\mathbf{Vc}$) at the transmitter side and post-processing to the received signal ($\mathbf{U}^H\mathbf{y}$) we obtain the relation

$$\begin{aligned} \mathbf{U}^H\mathbf{y} &= \mathbf{U}^H(\mathbf{U}\Sigma\mathbf{V}^H)\mathbf{V}\mathbf{c} + \mathbf{U}^H\mathbf{n} \\ \tilde{\mathbf{y}} &= \Sigma\tilde{\mathbf{c}} + \tilde{\mathbf{n}} \end{aligned} \tag{2.92}$$

where $\tilde{\mathbf{n}}$ is still Gaussian with the same variance than $\mathbf{n}$ and $||\tilde{\mathbf{c}}||^2 = ||\mathbf{c}||^2$, thus the power is unchanged.

Equation (2.92) represents the system as r equivalent parallel SISO Gaussian channels with signal powers given by the eigenvalues.

$$\tilde{y}_i = \sqrt{\lambda_i}\tilde{c}_i + \tilde{n}_i \qquad 1 \leq i \leq r \tag{2.93}$$

Thus, if the channel is perfectly known at the transmitter and the receiver, the transmitter can optimize its transmission strategy for each fading channel

realization. The ergodic capacity under the short power constraint, where the power associated with each channel realization must equal the average power constraint P, is given by

$$C(N_t, N_r) = \max_{\mathbf{Q}:\mathrm{tr}(\mathbf{Q})=P} B_W \log_2 \left(\det \left(\mathbf{I}_{N_r} + \frac{1}{N_0 B_W} \mathbf{H}\mathbf{Q}\mathbf{H}^H \right) \right) \tag{2.94}$$

where $\mathbf{Q}$ is the covariance of the MIMO channel input $\mathbf{Q} = \mathbb{E}(\mathbf{c}\mathbf{c}^H)$.

The capacity can be obtained as the sum of independent parallel channels capacities with the transmit power optimally allocated between these channels. We have

$$C(N_t, N_r) = \sum_{i=1}^{r} B_W \log_2 \left(1 + \frac{P_i}{N_0 B_W} \lambda_i \right) \tag{2.95}$$

where the power allocation is obtained by waterfilling

$$\frac{P_i}{P} = \begin{cases} \frac{1}{\gamma_0} - \frac{N_0 B_W}{\lambda_i P} & \frac{\lambda_i P}{N_0 B_W} \geq \gamma_0 \\ 0, & \frac{\lambda_i P}{N_0 B_W} < \gamma_0 \end{cases} \tag{2.96}$$

with the cutoff value γ_0 chosen to satisfy the total power constraint $\sum_{i=1}^{r} P_i = P$.

If the channel is unknown at the transmitter and perfectly known at the receiver, the power should be uniformly distributed over the transmit antennas. The instantaneous capacity can be obtained as

$$C(N_t, N_r) = \sum_{i=1}^{r} B_W \log_2 \left(1 + \frac{P}{N_t N_0 B_W} \lambda_i \right) \tag{2.97}$$

The instantaneous capacity of a (N_t, N_r) MIMO system can also be given using the well-known "logdet" equation [12, 49] as

$$C(N_t, N_r) = B_W \log_2 \det \left(\mathbf{I}_{N_r} + \frac{P}{N_t N_0 B_W} \mathbf{H}\mathbf{H}^H \right) \tag{2.98}$$

From the capacity in (2.97) and (2.98), we introduce two other capacities: the ergodic capacity and the outage capacity.

The channel capacity of a (N_t, N_r) MIMO system in ergodic channel environment can also be given by [12, 49] as

$$C(N_t, N_r) = \mathbb{E}_{\mathbf{H}} \left\{ B_W \log_2 \det \left(\mathbf{I}_{N_r} + \frac{P}{N_t N_0 B_W} \mathbf{H}\mathbf{H}^H \right) \right\} \tag{2.99}$$

Like the instantaneous capacity, the ergodic capacity is given in bits per second.

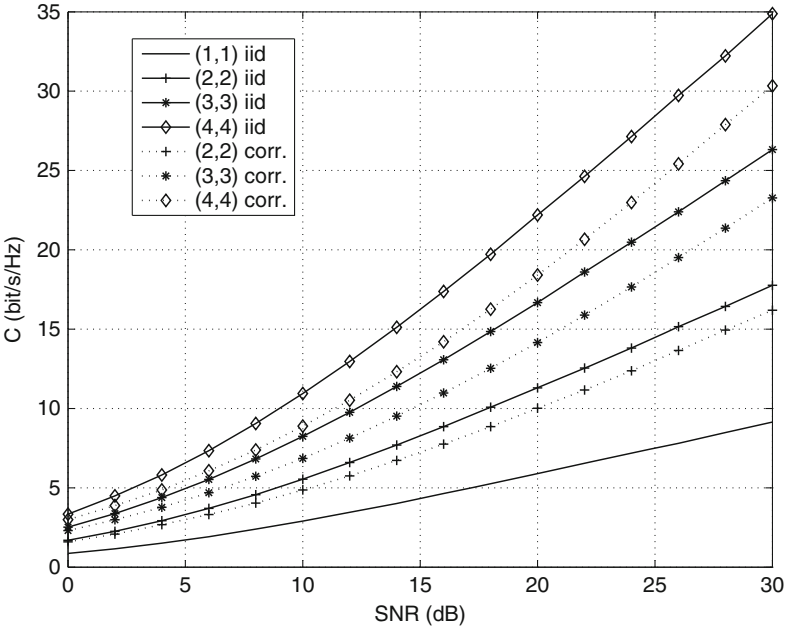

Fig. 2.15 The ergodic capacity for different antenna configurations in correlated and uncorrelated flat fading channels

Figure 2.15 shows the ergodic capacity of several MIMO configurations as a function of SNR over nonselective channels, i.i.d. according to the Rayleigh distribution. We can check that the capacity increases linearly with $\min(N_t, N_r)$ (each increase of 3 dB imply $\min(N_t, N_r)$ more bit/s/Hz). We also give the capacities obtained using correlated MIMO channels. We consider an uplink channel using linearly space antennas. At the transmitter side, the distance between the antennas is 0.5λ; the AoD is 20°. At the receiver side, the distance between the antennas is 4.0λ, the AoA as 20° and the AS as 5° which corresponds to an uplink case. The capacity improves by increasing the number of transmit and receive antennas and also SNR. The correlation between the MIMO channels decreases the capacity such as at 20 bps/Hz $(4, 4)$; MIMO system needs 18 dB and 22 dB in the independent and correlated channel environment, respectively.

If the duration of the block is limited compared to the coherence time of the MIMO channels, the capacity is treated as a random variable which depends on the instantaneous channel response and remains constant during the transmission of the block of data. If the channel capacity is below the outage capacity, there is no possibility that the transmitted block of information can be decoded with no errors.

The outage capacity, $C_{out}(q)$, is defined as the information rate that is guaranteed for $(100 - q)\%$ of the channel realizations. We have

$$Pr(C \leq C_{out}(q)) = q\% \tag{2.100}$$

2.4.3 Gain of MIMO Systems

MIMO systems can extract various gains considering that the channel is known or unknown at the transmitter side. If the channel is unknown at the transmitter, diversity and multiplexing gain can be achieved by MIMO systems. If the transmitter has the knowledge of channel information using feedback, array gain can also be provided by MIMO systems. We will summarize these gains in the following sections.

2.4.3.1 Array Gain

Considering the single input multiple output (SIMO) system with one transmit and N_r receive antennas, if the channel is known to the receiver, appropriate signal processing techniques can be applied to combine the received signal coherently so that the resultant power of the signal at the receiver is enhanced, leading to an improvement in signal quality. The average increase in received signal power at the receiver, $\mathbb{E}[\|\mathbf{h}\|^2]$, is defined as array gain which is proportional to the number of receive antennas. Array gain can also be exploited in systems with multiple antennas at the transmitter using linear or nonlinear precoding. Extracting the maximum possible array gain in such systems requires channel knowledge at the transmitter, so that the signals may be optimally processed before transmission. The array gain in MIMO systems depends on the number of transmit and receive antennas and is a function of the dominant singular value of the channel matrix.

2.4.3.2 Diversity Gain

As we mentioned before, the signal power in wireless channel fluctuates or fades with time, frequency and space. Diversity is used in wireless systems to combat fading. The basic idea behind diversity is to provide the receiver with several replicas over independently fading links (or diversity branches). As the number of the diversity branches increases, the probability that at any instant of time, one or more branch is not in a fade increases. Thus, diversity helps to stabilize a wireless link.

Diversity is available in SISO links in the form of time, such as channel coding in conjunction with interleaver or frequency diversity at the cost of data rate reduction due to the utilization of more time or more bandwidth. The introduction of multiple antennas at the transmitter and/or receiver provides spatial diversity. Compared to time and frequency diversity, spatial diversity does not incur a penalty in the data rate. The spatial diversity gain in the system is characterized by the number of independently fading diversity branches. The receive diversity can be obtained by using more than one antenna at the receiver and combining the independent signals at each receive antenna. In order to extract transmitter diversity, a suitable design

of the transmitted signal is required using STC or precoding scheme. The overall spatial diversity gain d of a MIMO system is defined by

$$d = -\lim_{\text{SNR}\to\infty} \frac{\log P_e(\text{SNR})}{\log \text{SNR}} \tag{2.101}$$

The spatial diversity gain describes how fast error probability decays with SNR since $P_e \propto SNR^{-d}$. The maximum spatial diversity order is $N_t \times N_r$.

2.4.3.3 Multiplexing Gain or Degrees of Freedom

When the path gains between individual transmit-receive antenna pairs fade independently, the channel matrix is well conditioned with high probability. Consequently, by transmitting independent information streams in parallel through the spatial channels, the data rate can be significantly increased. This effect is known as multiplexing gain and represents the increase in channel capacity. The multiplexing gain or degrees of freedom (DoF) r is defined as

$$r = \lim_{\text{SNR}\to\infty} \frac{R(\text{SNR})}{\log \text{SNR}}. \tag{2.102}$$

Multiplexing gain is the pre-log of the rate in the high-SNR regime and determines how fast rate increases with SNR. In a point to point MIMO system, the multiplexing gain is limited by $\min(N_t, N_r)$ that is the degree of freedom of this communication channel.

2.4.4 Diversity Multiplexing Tradeoff

Zheng and Tse [57] have proved that there exists a tradeoff between diversity gain and multiplexing gain for a slow fading channel. For a MIMO system with N_t transmit and N_r receive antennas, the optimum tradeoff curve, $d(r)$, has been evaluated in [57]. Assuming that the block size is equal or bigger than $N_t + N_r - 1$, the optimal tradeoff curve $d(r)$ is given by the piece-wise linear function connecting the points $(r, d(r))$; $\quad r = 0, \ldots, \min(N_t, N_r)$ where

$$d(r) = (N_t - r)(N_r - r). \tag{2.103}$$

This is a fundamental tradeoff which shows that it is not possible to reach at the same time the maximum diversity gain and maximum multiplexing gain. The DMT can be used to evaluate and compare the MIMO schemes. The function $d(r)$ is plotted in Fig. 2.16.

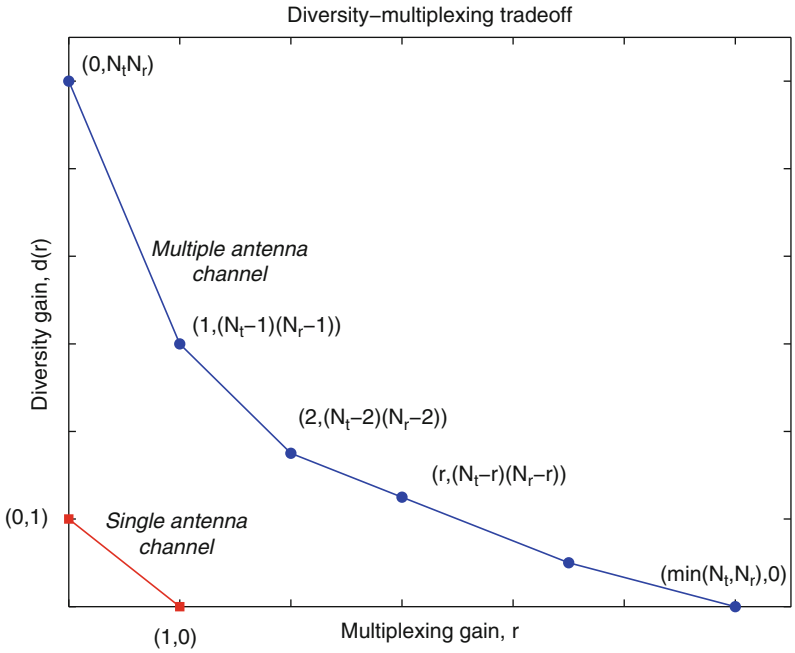

Fig. 2.16 Diversity-multiplexing tradeoff, $d(r)$ for general N_t, N_r

2.4.5 MIMO Codes

For a MIMO wireless transmission system, we consider a communication link with N_t transmit antennas and N_r receive antennas.

At the transmitter, information symbols s belonging to the constellation set Λ_s are parsed into blocks $\mathbf{s} = [s_1 \quad s_2 \quad \dots \quad s_Q]^T$ of size $Q \times 1$ in the symbol vector where Q is the number of information symbols. The MIMO encoder performs the mapping of the vector $\mathbf{s}$ to the matrix code $\mathbf{C}$ of size $N_t \times T$:

$$\mathbf{C} = \begin{bmatrix} c_{1,1} & \cdots & c_{1,T} \\ \vdots & \ddots & \vdots \\ c_{N_t,1} & \cdots & c_{N_t,T} \end{bmatrix} \tag{2.104}$$

where T is the number of time intervals that the information symbols are transmitted in the code matrix. Then, the T columns of $\mathbf{C}$ are sent through the N_t transmit antennas simultaneously. Each symbol in the code matrix belongs to constellation set Λ_c which may be identical or different than Λ_s depending on the code structure. Since Q information symbols are sent from each transmit antenna in T time intervals, the transmission rate of MIMO code is equal to $R_{\text{MIMO}} = Q/T$.

Assuming that the channel is flat fading, the signal from receive antenna j at time t is a noisy superposition of transmitted signals from N_t transmit antennas as

$$y_{j,t} = \sum_{i=1}^{N_t} h_{j,i,t} c_{i,t} + n_{j,t}, \tag{2.105}$$

where $h_{j,i,t}$ is the complex channel coefficient from transmit antenna j to receive antenna i at time t and $n_{j,t}$ is the additive noise which is modeled as independent samples of a zero-mean complex Gaussian random variable.

Considering the quasi-static flat fading channels ($h_{ji,t} = h_{ji}$ for $1 \leq t \leq T$), the channel coefficient matrix $\mathbf{H}$ with the dimension of $N_r \times N_t$ is denoted as

$$\mathbf{H} = \begin{bmatrix} h_{1,1} & \dots & h_{1,N_t} \\ \vdots & \ddots & \vdots \\ h_{N_r,1} & \dots & h_{N_r,N_t} \end{bmatrix}. \tag{2.106}$$

Then, the received signal in (2.105) can be written with a matrix form as

$$\mathbf{Y} = \mathbf{HC} + \mathbf{N}, \tag{2.107}$$

where $\mathbf{Y}$ and $\mathbf{N}$ are the received and noise matrices, respectively, with the dimension of $N_r \times T$. Given $\mathbf{Y}$, the MIMO decoder decodes $\mathbf{s}$ using the unique mapping between $\mathbf{C}$ and $\mathbf{s}$.

There are two main techniques which exploit the potential benefits of MIMO channel: spatial multiplexing (SM), which can be regarded as a special class of STC where streams of independent data are transmitted over different antennas, thus maximizing the average data rate over the MIMO systems and STBC, which offers diversity and coding gains with improved spectral efficiency. In the next section, we shall describe the well-known MIMO schemes such as STBC codes and V-BLAST.

2.4.6 *Design Criteria for Space-Time Codes*

In this section, we will introduce the criteria to build efficient STC. We define the pairwise block error event for a realization of the channel $\mathbf{H}$, $\Pr(\mathbf{C} \rightarrow \mathbf{C}'|\mathbf{H})$ as the event that the receiver decodes the block $\mathbf{C}'$ erroneously when the block $\mathbf{C}$ is actually sent.

Defining the difference matrix

$$\mathbf{D} = \begin{bmatrix} c_{11} - c'_{11} & \dots & c_{1T} - c'_{1T} \\ c_{21} - c'_{21} & \dots & c_{2T} - c'_{2T} \\ \vdots & \ddots & \vdots \\ c_{N_t 1} - c'_{N_t 1} & \dots & c_{N_t 2} - c'_{N_t 2} \end{bmatrix} \tag{2.108}$$

Since the matrix $\mathbf{E} = \mathbf{D}\mathbf{D}^H$ is Hermitian of size $N_t \times N_t$, there exists a unitary matrix $\mathbf{T}$ and a real diagonal matrix $\mathbf{U}$ such as $\mathbf{T}\mathbf{E}\mathbf{T}^H = \mathbf{U}$. The elements of the diagonal of $\mathbf{U}$ are the eigenvalues of $\mathbf{A}$, i.e., $\lambda_i; i = 1, 2, .., N_t$.

We can show that the probability $P(\mathbf{C} \to \mathbf{C}'|\mathbf{H})$ can be upper bounded using the Chernoff bound:

$$Pr(\mathbf{C} \to \mathbf{C}'|\mathbf{H}) \leq \exp\left(-\frac{E_s}{4N_0N_t}d^2(\mathbf{C}, \mathbf{C}')\right) \tag{2.109}$$

$$\begin{aligned} d^2(\mathbf{C}, \mathbf{C}') &= \sum_{j=1}^{N_r} \mathbf{h}_j \mathbf{D}\mathbf{D}^H \mathbf{h}_j^H \\ &= \sum_{j=1}^{N_r} \mathbf{h}_j \mathbf{T}^H \mathbf{U}\mathbf{T}\mathbf{h}_j^H \\ &= \sum_{j=1}^{N_r} \sum_{i=1}^{N_t} \lambda_i ||\beta_{ij}||^2 \end{aligned}$$

where $\mathbf{h}_j = [h_{j1}\, h_{j2} \ldots h_{jN_t}]$ is the jth line of $\mathbf{H}$. β_{ij} is the ith element of the vector $\beta_j = \mathbf{h}_j \mathbf{T}^H$.

After averaging over the fading channels, we show that the pairwise error probability (PEP) $Pr(\mathbf{C} \to \mathbf{C}')$ can be upper bounded with

$$Pr(\mathbf{C} \to \mathbf{C}') \leq \left(\frac{E_s}{4N_tN_0}\right)^{-r_d N_r} \left(\prod_{k=1}^{r_d} \lambda_k\right)^{-N_r} \tag{2.110}$$

where r_d is the rank of the matrix $\mathbf{E}$ and λ_k corresponds to the nonzero eigenvalues of the difference matrix $\mathbf{D}$.

The aim is to build an optimal encoder minimizing the PEP $Pr\{\mathbf{C} \to \mathbf{C}'\}$ for all possible pairs [47].

From this expression, we define two criteria for the construction of the code: the rank criterion and the determinant criterion which determine, respectively, diversity and coding gain.

Rank Criterion: in order to achieve maximum diversity gain equal to N_tN_r, the difference matrix $\mathbf{D}$ has to be full rank over all pairs of distinct codewords. If the minimum rank is equal to r_d over all possible codewords, the diversity gain of r_dN_r is achieved.

Determinant Criterion: the term $\prod_{k=1}^{r_d} \lambda_k$ is the coding gain. It should be maximized over all pairs of distinct codewords.

The diversity criterion is the most important one of the two since it determines the slope of the performance curve in double-logarithmic scale.

If the difference matrix is of full rank, then the product of eigenvalues is equal to the determinant of matrix $\mathbf{E}$. In this case, the determinant criterion can be written as

$$c_g = \min_{\mathbf{C}\neq\mathbf{C}'} \left|\det[(\mathbf{C}-\mathbf{C}')(\mathbf{C}-\mathbf{C}')^H]\right|^{1/r_d} = \min_{\mathbf{C}\neq\mathbf{C}'} |\det \mathbf{E}|^{1/r_d}. \tag{2.111}$$

Trace Criterion: For small SNR and/or the high values of $r_d N_r$, in order to minimize the error probability in (2.110), the minimum sum of all eigenvalues $\sum_{r=1}^{r_d} \lambda_r$ of matrix $\mathbf{E}$ among all the pairs of distinct codewords should be also maximized.

Since $\mathbf{E}$ is a $N_t \times N_t$ matrix, the sum of all the eigenvalues is equal to the sum of the all elements on the main diagonal or the trace of $\mathbf{E}$ that can be expressed as

$$\sum_{r=1}^{r_d} \lambda_r = \mathrm{tr}(\mathbf{E}) = \sum_{i=1}^{N_t} E_{i,i}. \tag{2.112}$$

The trace of $\mathbf{E}$ can be also written as

$$\mathrm{tr}(\mathbf{E}) = \sum_{i=1}^{N_t} \sum_{t=1}^{T} |c_{i,t} - c'_{i,t}|^2, \tag{2.113}$$

Consequently, this criterion is equivalent to the maximization of the Euclidean distance between the pair of codewords $\mathbf{C}$ and $\mathbf{C}'$. This distance can be bounded by the minimum Euclidean distances of the signal constellations.

2.4.6.1 Orthogonal Space-Time Block Codes

Alamouti proposed a remarkable low complexity open loop transmit diversity scheme for $N_t = 2$ with $Q = 2$ and $T = 2$ [2]. Alamouti's code is the only complex orthogonal STBC that achieves maximum diversity with rate 1 allowing to reach the full capacity.

In this scheme, the input data stream is first mapped into symbols using a constellation mapper, and the symbol stream is then divided into two substreams. At a particular symbol period, the transmitted symbols from the first and second antenna are s_1 and s_2, respectively. In the next symbol period, the symbol transmitted from the first antenna is $-s_2^*$ and the symbol transmitted from the second antenna is s_1^*. Hence, we can write the code matrix as

$$\mathbf{C} = \begin{bmatrix} s_1 & -s_2^* \\ s_2 & s_1^* \end{bmatrix}. \tag{2.114}$$

Note that it is orthogonal since $\mathbf{C}\mathbf{C}^H = \left(|s_1|^2 + |s_2|^2\right)\mathbf{I}_2$.

Under the assumption that the channel is flat fading and constant over two consecutive symbol periods, the two received signals for $N_r = 1$ are given by

$$[y_{11} \quad y_{12}] = [h_{11} \quad h_{12}] \begin{bmatrix} s_1 & -s_2^* \\ s_2 & s_1^* \end{bmatrix} + [n_{11} \quad n_{12}]. \tag{2.115}$$

Defining the transmitted and received signal vectors as $\mathbf{S} = [s_1 \quad s_2]^T$ and $\mathbf{y_e} = [y_{11} \quad y_{12}^*]^T$, respectively, we can also write (2.115) in a matrix/vector form as

$$\begin{aligned} \mathbf{y_e} &= \begin{bmatrix} h_{11} & h_{12} \\ h_{12}^* & -h_{11}^* \end{bmatrix} \begin{bmatrix} s_1 \\ s_2 \end{bmatrix} + \begin{bmatrix} n_{11} \\ n_{12}^* \end{bmatrix} \\ &= \mathbf{H_e}\mathbf{s} + \mathbf{n_e} \end{aligned} \tag{2.116}$$

Note that the channel matrix has an orthogonal structure, ${\mathbf{H_e}}^H \mathbf{H_e} = G_{21}\mathbf{I}_2$, where $G_{21} = |h_{11}|^2 + |h_{21}|^2$ is the diversity gain.

Assuming that all the symbols are equiprobable, and since the noise vector $\mathbf{n_e}$ is assumed to be a multivariate AWGN vector, we can easily write the optimum maximum likelihood (ML) decoder as

$$\hat{\mathbf{s}} = \arg \min_{\mathbf{s} \in \Lambda_s^2} \|\mathbf{y_e} - \mathbf{H_e}\mathbf{s}\|^2. \tag{2.117}$$

Since $\mathbf{H_e}$ has an orthogonal structure, the ML decoding in (2.117) can be simplified considering the modified signal vector which is the multiplication of the Hermitian of the channel matrix by the received vector

$$\tilde{\mathbf{s}} = {\mathbf{H_e}}^H \mathbf{y_e} = G_{21}\mathbf{s} + \tilde{\mathbf{n}} \tag{2.118}$$

Since the noise vector $\tilde{\mathbf{n}} = {\mathbf{H_e}}^H \mathbf{n_e}$ is still zero-mean and covariance $\rho N_0 \mathbf{I}_2$, we can decode separately the two symbols.

In that case, the decoding is performed as

$$\hat{\mathbf{s}} = \arg \min_{\mathbf{s} \in \Lambda_s^2} \|\tilde{\mathbf{s}} - G_{21}\mathbf{s}\|^2. \tag{2.119}$$

Hence, by using this simple linear combining, the two-dimensional minimization problem in (2.119) is decoupled into two one-dimensional problems as

$$\hat{s_1} = \arg \min_{s_1 \in \Lambda_s} |\tilde{s_1} - G_{21}s_1|^2 \quad \text{and} \quad \hat{s_2} = \arg \min_{s_2 \in \Lambda_s} |\tilde{s_2} - G_{21}s_2|^2. \tag{2.120}$$

Compared to a SISO transmission, SNR for each symbol is $(|h_{11}|^2 + |h_{12}|^2)P/N_0B_W$. Hence a two branch diversity performance (diversity gain of order two) is obtained at the receiver.

For decoding, the $(2,1)$ STBC requires only two complex multiplications and one complex addition per symbol. Using 2^{M_c} constellation points, where M_c is the number of bits per symbol, this linear combining reduces the number of decoding metrics that has to be computed for ML decoding from 2^{2M_c} to 2^{M_c+1}. Furthermore, $(2,1)$ STBC can be easily extended to N_r receive antenna case. The diversity order provided by this scheme is $2N_r$.

The (N_t, N_r, T) STBC capacity is given by [12]

$$C(N_t, N_r, T) = \frac{1}{T}\mathbb{E}_{\mathbf{H_e}}\left\{B\log_2\det\left(\mathbf{I}_{N_rT} + \frac{P}{N_tN_0B_W}\mathbf{H_e}\mathbf{H_e}^H\right)\right\}. \tag{2.121}$$

In order to investigate the $(2,1)$ STBC capacity, we need to compute the mutual information between the transmitted and the received vectors $\mathbf{s}$ and $\mathbf{y_e}$ in the equivalent channel matrix $\mathbf{H_e}$ and compare it with the capacity of multiple antenna system with $N_t = 2$ and $N_r = 1$. Since $\mathbf{H_e}\mathbf{H_e}^H = \mathbf{H_e}^H\mathbf{H_e} = G_{21}\mathbf{I}_2$ for $N_r = 1$, the achievable capacity of this orthogonal STBC is

$$C = B\log_2\left(1 + \frac{P}{2N_0B_W}G_{21}\right) = C(N_t = 2, N_r = 1), \tag{2.122}$$

which indicates that $\mathbf{C}$ code can achieve the same channel capacity with the multiple antenna system for $N_t = 2$ and $N_r = 1$.

It is proven by the Hurwitz–Radon theorem that except the Alamouti code, there exist only few complex orthogonal STBC with rate less than the Alamouti code [48]. For example, for $N_t = 3$, $N_r = 1, Q = 3$ and $T = 4$ and consequently $R_{MIMO} = 3/4$ we have the following code matrix:

$$\mathbf{C}_{STBC,3} = \begin{bmatrix} s_1 & s_2 & s_3 & 0 \\ -s_2^* & s_1{}^* & 0 & -s_3 \\ -s_3^* & 0 & s_1{}^* & s_2 \end{bmatrix} \tag{2.123}$$

However, it is possible to achieve transmission rate 1 for complex constellations for more than two transmit antennas by sacrificing orthogonality.

2.4.6.2 Nonorthogonal Space-Time Block Codes

Non-orthogonal (NO) STBC have been proposed for three transmit antennas in [52] at different transmission rates and for four transmit antennas with transmission rate 1 in terms of capacity in [38] and diversity in [17] at the expense of performance loss. By sacrificing orthogonality, it is possible to build codes with rate one such as the quasi-orthogonal space-time codes (QO-STBC) [17, 38, 50]. The matrix code of the QO-STBC is given by

$$\mathbf{C}_{QO-STBC,4} = \begin{bmatrix} s_1 & -s_2^* & -s_3^* & s_4 \\ s_2 & {s_1}^* & -s_4^* & -s_3 \\ s_3 & -s_4^* & {s_1}^* & -s_2 \\ s_4 & s_3^* & {s_2}^* & s_1 \end{bmatrix} \tag{2.124}$$

This matrix is obtained from two Alamouti matrices and a Hadamard transform.

Defining the transmitted and received signal vectors as $\mathbf{S} = [s_1 \quad s_2 \quad s_3 \quad s_4]^T$ and $\mathbf{y_e} = [y_{11} \quad y_{12}^* \quad y_{13}^* \quad y_{14}]^T$, respectively, the input–output relation can be written as

$$\begin{aligned} \mathbf{y_e} &= \begin{bmatrix} h_{11} & h_{12} & h_{13} & h_{14} \\ h_{12}^* & -h_{11}^* & h_{14}^* & -h_{13}^* \\ h_{13}^* & h_{14}^* & -h_{11}^* & -h_{12}^* \\ h_{14} & -h_{13} & -h_{12} & h_{11} \end{bmatrix} \begin{bmatrix} s_1 \\ s_2 \\ s_3 \\ s_4 \end{bmatrix} + \begin{bmatrix} n_{11} \\ n_{12}^* \\ n_{13}^* \\ n_{14} \end{bmatrix} \\ &= \mathbf{H_e}\mathbf{s} + \mathbf{n_e} \end{aligned} \tag{2.125}$$

Compared to orthogonal codes, multiplying the received vector by ${\mathbf{H_e}}^H$ does not allow us to obtain the ML performance. Indeed, we have

$${\mathbf{H_e}}^H\mathbf{H_e} = \sum_{i=1}^{4}(|h_{1i}|^2)\mathbf{I}_4 + \mathbf{J} \tag{2.126}$$

where $\mathbf{J}$ is an interfering matrix composed of some nonzero elements given by

$$\mathbf{J} = \begin{bmatrix} 0 & 0 & 0 & \alpha \\ 0 & 0 & -\alpha & 0 \\ 0 & -\alpha & 0 & 0 \\ \alpha & 0 & 0 & 0 \end{bmatrix} \tag{2.127}$$

where $\alpha = 2\Re(h_{11}^* h_{14} - h_{12}^* h_{13})$. Since this code is not orthogonal,compared to the Alamouti code, linear decoding (ZF or MMSE) is no more optimal. In order to obtain the ML solution, we can apply sphere decoding.

Other nonorthogonal STBC such as the diagonal space-time (DAST) block codes [9] and threaded algebraic space-time (TAST) block codes [10] are using rotated modulations to achieve the optimal tradeoff between diversity, rate and delay.

2.4.6.3 V-BLAST

An architecture which theoretically achieves the capacity in an independent Rayleigh scattering environment was proposed as bell labs space time (BLAST) in [11]. Difficulties in the implementation of the original scheme led to a simplified

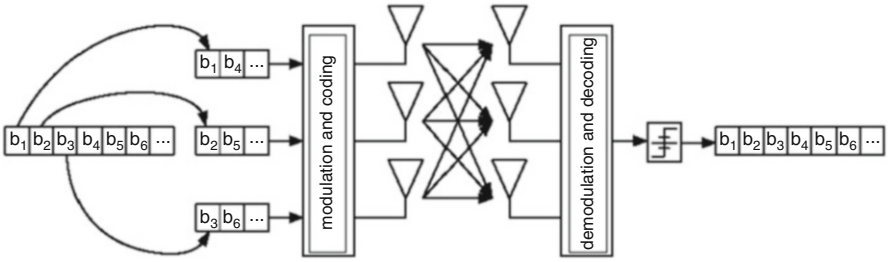

Fig. 2.17 V-BLAST scheme

architecture called V-BLAST [13,56] where each layer is associated with a certain transmit antenna as shown in Fig. 2.17.

As an example, we will consider the case with $N_t = N_r = 2$, $Q = 2$, $T = 1$ which provides the rate of $R_{MIMO} = 2$; the code matrix is given by

$$\mathbf{C}_{V-BLAST,2} = \begin{bmatrix} s_1 \\ s_2 \end{bmatrix} \tag{2.128}$$

where s_1, s_2 are obtained from the symbol constellation Λ_s.

Under the assumption that the channel is flat fading and constant over two consecutive symbol periods, the received signal is written in the matrix form as

$$\begin{bmatrix} y_{11} \\ y_{21} \end{bmatrix} = \mathbf{H} \begin{bmatrix} s_1 \\ s_2 \end{bmatrix} + \begin{bmatrix} n_{11} \\ n_{21} \end{bmatrix} \tag{2.129}$$

In this case we have $\mathbf{C} = \mathbf{s}$ and the relation (2.107) becomes the V-BLAST input–output relation

$$\mathbf{y} = \mathbf{H}\mathbf{s} + \mathbf{n} \tag{2.130}$$

where $\mathbf{s}$ is the transmit vector of size $N_t \times 1$ and $\mathbf{y}$ is the receive vector of size $N_r \times 1$.

In order to be able to decode, the system should be well conditioned: when $N_r \geq N_t$, the MIMO channel matrix should be full rank with high probability.

The optimum decoding method is ML decoding, where the receiver compares all possible combinations of symbols which could have been transmitted and results in the estimate

$$\hat{\mathbf{s}} = \arg \min_{\mathbf{s} \in \Lambda_s^{N_t}} \|\mathbf{y} - \mathbf{H}\mathbf{s}\|^2 . \tag{2.131}$$

The complexity of ML decoding becomes high when many antennas or higher-order modulations are used. Sphere decoding which avoids explicit exhaustive search [8] can be used to reduce the complexity of the ML decoding. If the number

of receive antennas is at least as large as the number of transmit antennas ($N_r \geq N_t$), there exists linear and nonlinear decoding schemes for V-BLAST.

The zero forcing (ZF) receiver consists in multiplying the received vector by the $N_s \times N_r$ pseudo-inverse matrix of $\mathbf{H}$

$$\tilde{\mathbf{y}} = \mathbf{G}\mathbf{y} = (\mathbf{H})^{\dagger}\mathbf{y} \tag{2.132}$$

where $\mathbf{A}^{\dagger}$ is the Moore–Penrose pseudo-inverse of $\mathbf{A}$.

The minimum mean square error (MMSE) receiver applies a $N_s \times N_r$ matrix to the received vector

$$\tilde{\mathbf{y}} = \mathbf{G}\mathbf{y} = \left[\mathbf{H}^H\mathbf{H} + \frac{N_t N_0 B_W}{P}\mathbf{I}_{N_t}\right]^{-1}\mathbf{H}^H\mathbf{y} \tag{2.133}$$

The nulling and cancelling (NC) algorithm [14] is a generalization of the decision-feedback algorithm. After having transformed the MIMO channel matrix into an upper triangular matrix, we estimate a first data, then remove its contribution before the estimation of the second one. After the QR decomposition of the channel matrix $\mathbf{H} = \mathbf{Q}\mathbf{R}$ where $\mathbf{Q}$ is an unitary matrix and $\mathbf{R}$ is an upper triangular matrix, we calculate the two following matrices:

$$\begin{cases} \mathbf{G} = \text{diag}^{-1}(\mathbf{R})\mathbf{Q}^H \\ \mathbf{L} = \text{diag}^{-1}(\mathbf{R})\mathbf{R} - \mathbf{I}_{N_r} \end{cases} \tag{2.134}$$

After multiplying the received vector by $\mathbf{G}$, we get the following relation:

$$\tilde{\mathbf{y}} = \mathbf{G}\mathbf{y} = \text{diag}^{-1}(\mathbf{R})\mathbf{R}\mathbf{s} + \mathbf{G}\mathbf{n} \tag{2.135}$$

Consequently, it is possible to estimate successively the symbols $\mathbf{s}_{N_t}, \mathbf{s}_{N_t-1}, \ldots, \mathbf{s}_1$:

$$\begin{cases} \hat{\mathbf{s}}_{N_t} & = \text{decision}\left((\tilde{\mathbf{y}})_{N_t}\right) \\ \hat{\mathbf{s}}_{N_t-1} & = \text{decision}\left((\tilde{\mathbf{y}})_{N_t-1} - \hat{\mathbf{s}}_{N_t}\mathbf{L}_{N_t-1,N_t}\right) \\ \vdots & \\ \hat{\mathbf{s}}_1 & = \text{decision}\left((\tilde{\mathbf{y}})_1 - \hat{\mathbf{s}}_{N_t}\mathbf{L}_{1,N_t} - \ldots - \hat{\mathbf{s}}_2\mathbf{L}_{1,2}\right) \end{cases} \tag{2.136}$$

The NC detection has been introduced using a ZF criterion but can be also applied to MMSE criterion. Furthermore, instead of choosing the natural ordering, it is better to decode starting from the most powerful symbol.

References

1. Agrawal D, Tarokh V, Naguib A, Seshadri N (1998) Space-time coded OFDM for high data-rate wireless communication over wideband channels. Proc. of Vehicular Technology Conference (VTC). 3 : 2232–2236
2. Alamouti S M (1998) A Simple Transmit Diversity Technique for Wireless Communications. IEEE Journal on Selec. Areas in Commun. 16 : 1451–1458
3. Bello P A (1963) Characterization of randomly time-varying linear channels. IEEE Transaction on Communications. 11 : 360–393
4. Bolcskei H, Paulraj A J (2000) Space-frequency coded broadband OFDM systems. Proc. of IEEE Wireless Communications and Networking Conference (WCNC). 1 : 1–6
5. Bolcskei H, Paulraj A J (2000) Performance of space-time codes in the presence of spatial fading correlation. Proceedings of IEEE Asilomar Conf. on Signals, Systems, and Computers. Pacific Grove, CA. 1 : 687–693
6. Brown T W C, Saunders S R, Stavrou S, Fiacco M(2007) Characterization of Polarization Diversity at the Mobile. IEEE Transactions on Vehicular Technology. 56 : 2440–2447
7. Clarke R H (1968) A statistical theory of mobile-radio reception. Bell System Technical Journal. 47 : 957–1000
8. Damen M O, Chkeif A, Belfiore J C (2000) Lattice code decoder for space time codes. IEEE Communication Letter. 4 : 161–163
9. Damen M O, Abed-Meraim K, Belfiore J C (2002) Diagonal Algebraic Space Time Block Codes. IEEE Trans. on Information Theory. 48: 628–636
10. El Gamal H, Damen M O (2003) Universal Space Time Coding. IEEE Trans. on Information Theory. 49 : 1097–1119
11. Foschini G J (1996) Layered space-time architecture for wireless communications in a fading environment when using multiple antennas. Bell Laboratories Technical Journal. 1 : 41–59
12. Foschini G J, Gans M J (1998) On the limits of wireless communications in fading environment when using multiple antennas. Wireless Personal Communications. 6 : 311–335
13. Foschini G J, Golden G D, Valenzuela R A, Wolniansky P W (1999) Simplified processing for high spectral efficiency wireless communication employing multi-element arrays. IEEE Journal on Selected Areas on Communications. 17 : 1841–1852
14. Golden G D, Foschini G J, Valenzuela R A, Wolniansky P W (1999) Detection algorithm and initial laboratory results using the V-BLAST space time communication architecture. Electronic Letters. 35 : 14–16
15. Goldsmith A (2005) Wireless Communications. Cambridge University Press.
16. Hong Z, Hughes B L (2002) Robust space-time codes for broadband OFDM systems, Proc. of IEEE Wireless Communications and Networking Conference (WCNC). 1 : 105–108
17. Jafarkhani H (2000) A quasi-orthogonal space-time block code. IEEE Transaction on Communication. 49 : 1–4
18. Jakes W C (1974) Microwave Mobile Communications. Wiley-IEEE Press. 2nd edition.
19. Kainulainen A, Vuokko L, Vainikainen P (2005) Polarization behavior in different urban radio environments at 5.3 GHz. COST 273, Tech. Rep. 05–018
20. Kermoal J P, Schumacher L, Mogensen P E, Pedersen K I (2000) Experimental investigation of correlation properties of MIMO radio channels for indoor picocell scenario. Proc. of Vehicular Technology Conference (VTC). Boston, USA. 1 : 14–21
21. Kermoal J P, Schumacher L, Pedersen K I, Mogenson P E, Frederiksen F (2002) A stochastic MIMO radio channel model with experimental validation. IEEE Journal on Selected Areas on Communications. 20 :1211–1226
22. Kozono S, Tsuruhara T, Sakamoto M (1984) Base station polarization diversity reception for mobile radio. IEEE Trans. Veh. Technol. 33: 301–306
23. Kyritsi P (2001) Propagation characteristics of horizontally and vertically polarized electric fields in an indoor environment: simple model and results, in Proc. IEEE Vehicular Technology Conference. 3 : 1422–1426

24. Lee W C Y, Yeh Y S (1972) Polarization diversity system for mobile radio. IEEE Transaction on Communications. 20 : 912–923
25. Lee K F, Williams D B (2000) A space-frequency transmitter diversity technique for OFDM systems. Proc. IEEE Global Telecommunications Conference (GLOBECOM). 3 : 1473–1477
26. Lee K F, Williams D B (2000) A space-time coded transmitter diversity technique for frequency selective fading channels. Proceedings of Sensor Array and Multichannel Signal Processing Workshop. 149–152
27. Le Floch, Alard M, Berrou C (1995) Coded orthogonal frequency division multiplex. Proceedings of the IEEE. 83 : 982–996
28. Lempiainen J J A, Laiho-Steffens J K (1998) The Performance of Polarization Diversity Schemes at a Base Station in Small/Micro Cells at 1800 MHz. IEEE Transactions on Vehicular Technology. 47 : 1087–1092
29. Loredo S, Manteca B, Torres R (2002) Polarization diversity in indoor scenarios: an experimental study at 1.8 and 2.5 GHz. Proc. of IEEE International Symposium on Personal, Indoor and Mobile Radio Communications (PIMRC). 2 : 896–900
30. Lotse F, Berg J E, Forssen U, Idahl P (1996) Base station polarization diversity reception in macrocellular systems at 1800 MHz. Proc. IEEE Vehicular Technology Conference. 1643–1646
31. Lu B, Wang X (2000) Space-time code design in OFDM systems. Proc. IEEE Global Telecommunications Conference (GLOBECOM). 2 :1000–1004
32. Molisch A F (2011) Wireless Communications. John Wiley, 2nd edition
33. Motorola (2002) Polarization effects and Path statistics for the spatial channel model, SCM-055, SCM Ad-hoc meeting.
34. Nabar R U, Bölcskei H, Erceg V, Gesbert D, Paulraj A J (2002) Performance of Multiantenna Signaling Techniques in the Presence of Polarization Diversity, in IEEE transactions on signal processing. 50 : 2553–2562
35. Naguib A, Tarokh V, Seshadri N, Calderbank A R (1998) A space-time coding modem for high-data-rate wireless communications. IEEE Journal on Selected Areas on Communications. 16 : 1459–1478
36. Oestges C, Clerckx B, Guillaud M, Debbah M (2008) Dual-polarized wireless communications: from propagation models to system performance evaluation. IEEE Trans. Wireless Commun. 7 : 4019–4031
37. Ozcelik H, Herdin M, Weichselberger W, Wallace J, Bonek E (2003) Deficiencies of Kronecker MIMO Radio Channel Model. Electronics Letters. 39 : 1209–1210
38. Papadias C B, Foschini G J (2001) A Space-time coding approach for systems employing four transmit antenna. Proceedings of IEEE International Conference on Acoustics Speech and Signal Processing (ICASSP). 4 : 2481–2485
39. Pedersen K I, Mogensen P E, Fleury B H (2000) A stochastic model of the temporal and azimuthal dispersion seen at the base station in outdoor propagation environments, IEEE Trans. Veh. Technol. 49 : 437–447
40. Proakis J G (2001) Digital communications. McGraw-Hill,Boston,USA, 4^{th} edition.
41. Rappaport T S (1996) Wireless Communications: Principles and Practice. Upper Saddle River, Prentice Hall.
42. Saleh A A M, Valenzuela R A (1987) A statistical model for indoor multipath propagation. IEEE Journal on Selected Areas in Communications. 5 : 128–137
43. Sayeed A M (2002) Deconstructing multiantenna fading channels, IEEE Trans. Signal Processing 5 : 856–866
44. Schumacher L, Pedersen K I, Mogenson P E (2002) From antenna spacings to theoretical capacities - guidelines for simulating MIMO systems. Proceedings of IEEE PIMRC. 2 : 587–592
45. Steinbauer M, Molisch A F, Bonek E (2001) The doubledirectional radio channel. IEEE Antennas and Propagation Magazine. 43 : 51–63
46. Svantesson T, Jensen M A, Wallace J W (2004) Analysis of electromagnetic field polarizations in multiantenna systems. IEEE Transactions on Wireless Communications. 3 : 641–646

47. Tarokh V, Seshadri N, Calderbank A R (1998) Space-time codes for high data rate wireless communication: Performance criterion and code construction. IEEE Transaction on Information Theory. 44 : 744–765
48. Tarokh V, Jafarkhani H, Calderbank A (1999) Space-time block codes from orthogonal designs. IEEE Transaction on Information Theory. 45 : 1456–1467
49. Telatar E (1995) Capacity of multiple antenna Gaussian channels. AT&T Bell Laboratories, *Technical Report*
50. Tirkkonen O, Boarius A, Hottinen A (2000) Minimal nonorthogonality rate 1 space-time block code for 3+ Tx antennas. in Proc. of IEEE International Symposium on Spread Spectrum Techniques and Applications (ISSSTA). 2 : 429–432
51. Tse D, Viswanath P, Fundamentals of Wireless Communication, Cambridge University Press.
52. Uysal M, Georghiades C N (2002) Non-Orthogonal Space-Time Block Codes for 3TX Antennas. IEE Electronics Letters. 38 : 1689–1691
53. Vaughan R G (1990) Polarization diversity in mobile communications. IEEE Transactions on Vehicular Technology. 39 : 177–186
54. Wallace J, Jensen M, Modeling the Indoor MIMO Wireless Channel (2002) IEEE Trans. on Antennas and Propagation. 50 : 591–599
55. Weichselberger W, Herdin M, Ozcelik H, Bonek E (2006) A Stochastic MIMO Channel Model with Joint Correlation of Both Link Ends. IEEE Trans. Wireless Commun. 5 : 90–100
56. Wolniansky P W, Foschini G J, Golden G D, Valenzuela R A (1998) V-BLAST : An architecture for realizing very high data rates over rich-scattering wireless channel. Proceedings of URSI International Symposium on Signals, Systems, and Electronics. 1 : 295–300
57. Zheng L, Tse D (2003) Diversity and multiplexing: A fundamental tradeoff in multiple antenna channels, IEEE Trans. on Information Theory. 49 : 1073–1096

http://www.springer.com/978-1-4614-7740-2

Feedback Strategies for Wireless Communication

Özbek, B.; Le Ruyet, D.

2014, XVII, 332 p. 105 illus., 51 illus. in color.,
Hardcover
ISBN: 978-1-4614-7740-2